

$^{40}\text{Ar}/^{39}\text{Ar}$ study of plagioclases from the Rogaland anorthosite complex (SW Norway); an attempt to understand argon ages in plutonic plagioclase

A. Boven^{a,*}, P. Pasteels^a, S.P. Kelley^b, L. Punzalan^a, B. Bingen^c, D. Demaiffe^d

^a *Laboratory of Geochronology, Vrije Universiteit Brussel, Pleinlaan 2, 1050 Brussel, Belgium*

^b *Department of Earth Sciences, Open University, Milton Keynes MK7 6AA, UK*

^c *Norges Geologiske Undersøkelse, Leiv Eirikssons vei 39, 7040 Trondheim, Norway*

^d *Géochimie isotopique et Géodynamique Chimique, Université Libre de Bruxelles, CP160/02, av. F. Roosevelt 50, 1050 Bruxelles, Belgium*

Received 25 May 1999; accepted 16 August 2000

Abstract

The combined use of stepwise-heating and UV-laser ablation $^{40}\text{Ar}/^{39}\text{Ar}$ techniques with microprobe analyses on plutonic plagioclase allows the investigation of complex argon release and retention. The complexity arises from the multiphase nature of the samples comprising plagioclase, K-feldspar (in antiperthite), secondary “sericite” and various inclusions, in which some of the components also exhibit variable ages.

Fragments of plagioclase megacrysts and plagioclase separates from whole rock samples were selected from a well-constrained series of anorthosite–leuconorite intrusions of the Rogaland Igneous Complex (SW Norway) intruded at ca. 930 Ma. All samples exhibit saddle-like staircase-shaped argon-release spectra. Ages rise from around 400–600 to 750–900 Ma, though three samples exhibit excess argon released at high temperatures. The most remarkable aspect of this data is, however, the apparently linear correlation of $^{40}\text{Ar}^*/^{39}\text{Ar}$ with Ca/K. The stepwise-heating data reveal late stage cooling ages, considerably younger than the intrusive age and low temperature reheating of the Rogaland Igneous Complex during Caledonian overthrusting. Arrhenius plots for the stepwise heated samples show a linear trend of diffusion data at low temperatures followed by a systematic break around 900–1060°C.

Single spot ages obtained using a UV-laser show extreme age variations with heterogeneous excess argon contained in inclusions but no correlation of $^{40}\text{Ar}^*/^{39}\text{Ar}$ with Ca/K. This lack of correlation indicates that the two-component mixing model (with two end-members of distinct ages), suggested by the stepwise-heating data, is an artefact resulting from a more complex mechanism of argon release. The most apparent interpretation of this data is that both plagioclase and another potassium-rich minor component, probably K-feldspar antiperthite yield variable but correlated ages. Because the excess argon is found exclusively in samples from marginal leuconorite bodies and never in the core of the megacrysts, it is probably derived from the outgassing of the K-rich country rock. © 2001 Elsevier Science B.V. All rights reserved.

Keywords: Ar-40/Ar-39; Plagioclase; Laser; Ablation; Anorthosite; Southern Norway

* Corresponding author. Fax: +32-2-6293635.

E-mail address: aaboven@vub.ac.be (A. Boven).

1. Introduction

Among the feldspars, plagioclase is probably the most challenging mineral for $^{40}\text{Ar}/^{39}\text{Ar}$ dating. It has low K concentrations (0.05–0.5%) and, therefore, requires larger laser ablation craters so as to attain sufficient analytical precision, and is sensitive to the interference with minor K-rich impurities. Its retentivity for argon is not well understood and it occasionally yields discordant age spectra, which are not always easily interpreted. Saddle-shaped argon-release spectra have long been interpreted as indicating excess argon (Lanphere and Dalrymple, 1976; Harrison and McDougall, 1981) and the causes have been debated though some were shown to be a result of contamination (Lo Bello et al., 1987). Recently, Esser et al. (1997) and Singer et al. (1998) have shown the important effects of melt inclusions and the incorporation of older plagioclase grains into volcanic samples.

Despite all these pitfalls, $^{40}\text{Ar}/^{39}\text{Ar}$ dating of plagioclase has become an increasingly significant tool to constrain the timing of volcanism and contribute to the calibration of the paleomagnetic record and the astronomical time scale (Singer and Pringle, 1996) and has even been used to constrain cooling histories of plutons (Yu and Morse, 1992). At first sight, plagioclase may supposedly have a better stability during in vacuo laboratory heating experiments, compared to that of hydrous minerals such as hornblende and micas, which undergo reaction and physical change. But as demonstrated by Parsons et al. (1999) microtextures of alkali feldspars (deuteric, strain-controlled, fluid inclusions, etc.) are unstable during stepwise-heating experiments. It can be assumed that plagioclase will have a similar behaviour, considerably restricting the use of this mineral to decipher thermal histories. On the other hand, because of its low K concentration levels, plagioclase may be suitable to trace the effects of K-migration under natural conditions.

Our main aim is the investigation of Ar and K migration in plutonic plagioclase from a well-known case sufficiently deciphered during previous field, petrographic and geochronological studies. Plutonic plagioclase has been separated for the purpose from various anorthosite intrusions of the Rogaland Igneous Complex, South Norway of Sveconorwegian

(= Grenvillian) age. Stepwise-heating and UV-laser ablation $^{40}\text{Ar}/^{39}\text{Ar}$ dating results have been compared with microprobe analyses; Arrhenius plots have been calculated from the cumulative ^{39}Ar released during stepwise heating to countercheck whether the multiple diffusion domain (MDD)-model (Lovera et al., 1989) could explain the argon release from plutonic plagioclases. During a preliminary investigation on plagioclases from the Rogaland Igneous Complex (RIC) (Boven et al., 1996), stepwise-heating argon-release spectra were interpreted as resulting from a multiphase composition and not from diffusive argon loss, inferring an inhomogeneity in the K-distribution. UV-laser ablation $^{40}\text{Ar}/^{39}\text{Ar}$, microprobe analyses and additional $^{40}\text{Ar}/^{39}\text{Ar}$ stepwise heating on additional samples have been performed to refine these earlier interpretations and to check for inhomogeneity in the K-distribution within the plagioclase samples.

Numerous isotopic studies (Pasteels and Michot, 1975; Pasteels et al., 1979; Wielens et al., 1981; Verschure et al., 1980; Schärer et al., 1996; Bingen and van Breemen, 1996, 1998; Bingen et al., 1998a) provide a concise time frame for the magmatic emplacement and subsequent cooling of the RIC and resulting contact metamorphism superimposed on a regional Sveconorwegian metamorphism. $^{40}\text{Ar}/^{39}\text{Ar}$ results obtained on these plutonic plagioclases provide not only insights into $^{40}\text{Ar}/^{39}\text{Ar}$ systematics of plagioclase but also into the cooling history of the RIC.

2. Temporal constraints

2.1. Magmatic emplacement and cooling of the RIC

The RIC of Southwestern Norway (Fig. 1) is composed of three massif-type anorthosite intrusions (Egersund-Ogna, Håland-Helleren and Åna-Sira), a folded layered intrusion (Bjerkreim-Sokndal lopolith) consisting of a whole sequence from anorthosite-leuconorite-norite through mangerite and charnockite, to marginal leuconorite intrusions (Hydra and Garsaknatt). A stockwork of dykes of mainly jotunitic (monzonoritic) composition crosscuts the anorthosite

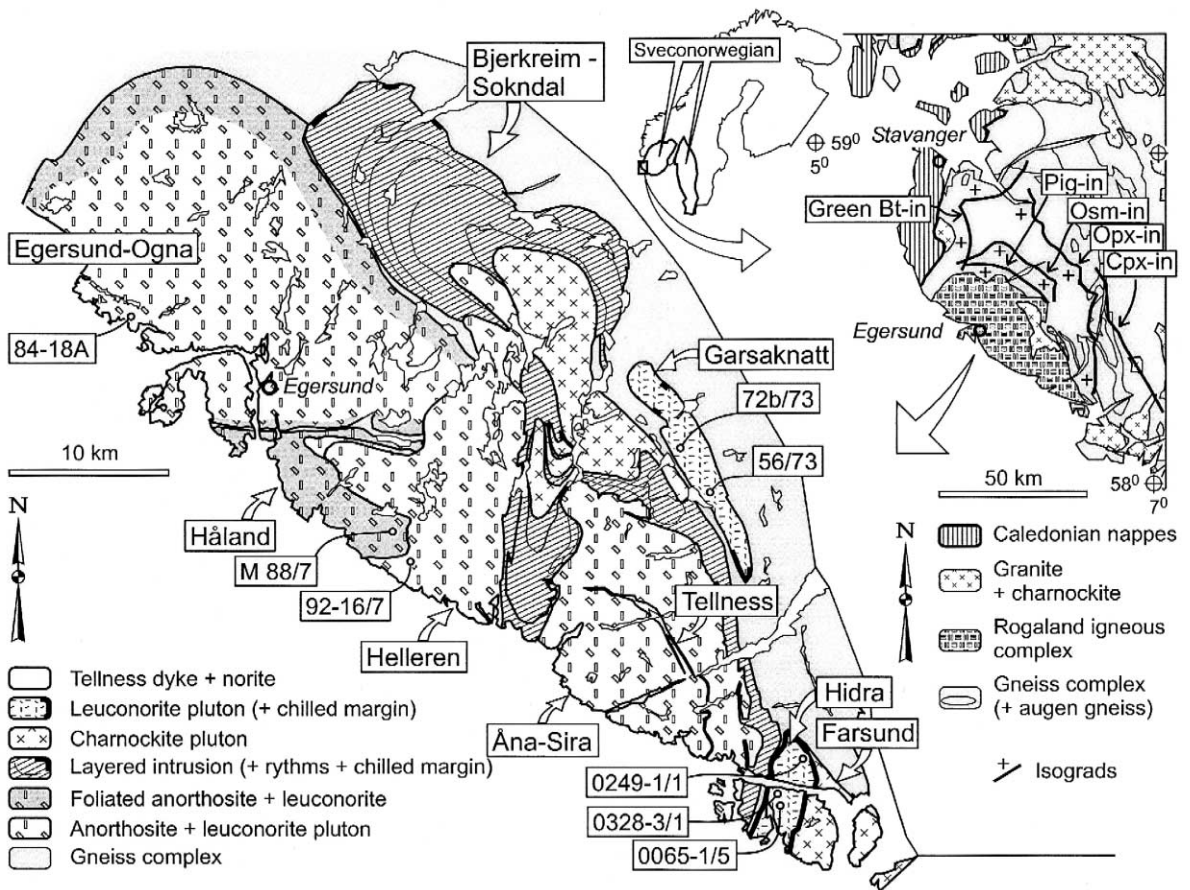


Fig. 1. Geological sketch map of Southwest Norway (Sigmond et al., 1984) and the Rogaland complex (Michot and Michot, 1969; Duchesne et al., 1985a) with isograds (Tobi et al., 1985), names of major units and sample location of analyzed plagioclases.

bodies and the lopolith. Charnockite bodies occur at the top of the Bjerkreim-Sokndal lopolith, or at the SE margin of the complex (Farsund charnockite); they are considered to belong to the same magmatic province (Michot and Michot, 1969; Duchesne et al., 1985a).

The massif-type anorthosite plutons formed under polybaric conditions. Al-rich orthopyroxene megacrysts crystallised at high pressure (9–15 kbar); the plagioclase-rich crystal mush rose in the crust to its final emplacement depth of about 5 kbar (Fram and Longhi, 1992; Longhi et al., 1993), leading to syn-emplacement deformation in the margin of the Egersund-Ogna intrusion (Fig. 1) (Duchesne et al., 1985b).

Field relations show that the Bjerkreim-Sokndal, Hydra and Garsaknatt bodies were emplaced after the anorthosite plutons. The best estimate of the time elapsed between these successive intrusive phases is provided by geochronology although the high crystallisation temperatures (1250–1100°C) (Fram and Longhi, 1992) make the distinction between times of crystallisation and cooling ambiguous. Moreover, equating crystallisation time and emplacement time is misleading in anorthosite bodies with polybaric assemblages.

A fine-grained border facies of jotunitic composition is observed at the contacts of the Hydra and Garsaknatt bodies and locally also at Bjerkreim-Sokndal. These facies have been interpreted as chilled

margins (Demaiffe and Hertogen, 1981; Duchesne and Hertogen, 1988; Duchesne et al., 1974; Robins et al., 1997), suggesting a fast cooling rate of the plutons just after intrusion and a significant difference in temperature between the intrusions and the host rocks.

Different units of the igneous complex yield consistent U–Pb zircon and baddeleyite ages of 930–920 Ma (Pasteels et al., 1979; Schärer et al., 1996) interpreted as crystallisation ages. Zircons separated from clusters of orthopyroxene megacrysts of the Egersund-Ogna, Hellenen and Åna-Sira anorthosites are tightly grouped with ages of 929 ± 2 , 932 ± 3 and 932 ± 3 Ma, respectively, indicating that a major magmatic pulse took place at 931 ± 2 Ma (Schärer et al., 1996).

2.2. Metamorphism in the country rocks

The emplacement and cooling of the RIC certainly influenced the mineral equilibria of the adjacent country rocks. The relative importance of this “contact metamorphism” effect and its superimposition or combination with the regional Sveconorwegian metamorphism remains however difficult to decipher.

Amphibolite- to granulite-facies regional metamorphism is bracketed between 1030 and 990 Ma (U–Pb data on zircon and monazite; Pasteels and Michot, 1975; Wielens et al., 1981; Bingen and van Breemen, 1998). Although this metamorphism induced penetrative deformation, Maijer (1996) noted that the granulite-facies metamorphism appears to be static. Contact metamorphism related to the RIC is associated with limited formation of monazite at 930–923 Ma (Bingen and van Breemen, 1998).

Regional cooling following the intrusion of the anorthosites is recorded by U–Pb titanite ages of amphibolite- to granulite-facies calc-alkaline augengneisses (Bingen and van Breemen, 1996): 12 samples yield a weighted average of 918 ± 2 Ma. This figure implies a homogeneous regional cooling to approximately 650–720°C (closure temperature range for titanite after Pidgeon et al., 1996; Zhang and Schärer, 1996) at ca. 920 Ma, i.e. about 10 Ma after anorthosite emplacement. Hornblende $^{40}\text{Ar}/^{39}\text{Ar}$ ages

(Bingen et al., 1998a) allow further evaluation of the regional cooling history. In pyroxene-rich samples (granulite-facies zone), located close to the RIC, $^{40}\text{Ar}/^{39}\text{Ar}$ hornblende ages (ca. 916 Ma) are essentially the same as titanite U–Pb ages. In biotite- and amphibole-rich samples (amphibolite-facies zone), the hornblende ages are significantly younger (ca. 871 Ma). That titanite and hornblende provide the same cooling ages in metamorphic terranes is unexpected since their reported closure temperatures range from 650–720°C (Zhang and Schärer, 1996) to 550–500°C (Harrison and McDougall, 1981), respectively. The U–Pb ages on titanite may, however, correspond to recrystallisation ages and not cooling ages (Zhang and Schärer, 1996).

2.3. Post-magmatic evolution of the RIC

Further cooling of the RIC proceeded much more slowly and affected the whole Sveconorwegian crustal segment leading to biotite-hornblende cooling ages around 870 Ma. The RIC has subsequently been affected by a mild Caledonian overprinting. The Sveconorwegian basement has been overthrust by a Caledonian nappe system ca. 4 km from the north-western contact of the Egersund-Ogna anorthosite body (Fig. 1, inset). In a ca. 6-km-wide zone along the front, the basement rocks display a secondary greenschist-facies metamorphic assemblage (development of green biotite) (Sauter et al., 1983; Verschure et al., 1980). The metamorphism decreased in intensity eastward to reach the pumpellyite–prehnite–quartz facies.

Secondary green biotite is formed upon metamorphic reaction at about 400°C and provides ca. 400 Ma Rb–Sr ages and 450 to 550 Ma K–Ar apparent ages (Verschure et al., 1980). This age difference is attributed to incorporation of ^{40}Ar released during metamorphism. Outside the green biotite-in isograd, brown Sveconorwegian biotites yield consistent ages of about 870 Ma by both Rb–Sr and K–Ar methods (Verschure et al., 1980). To the west of this isograd, two biotites coexist, brown biotite is locally affected and retrogressed to green biotite, chlorite and sagenite needles. In this zone, the K–Ar and $^{40}\text{Ar}/^{39}\text{Ar}$ ages on the brown biotite range from about 870 to 700 Ma, pointing to a varying degree of resetting.

The RIC was intruded by the subvolcanic basaltic Egersund dyke swarm at 616 ± 3 Ma (baddeleyite U–Pb age, Bingen et al., 1998b), which exhibit glassy margins, in some cases, indicating that the crystalline basement of SW Norway was eroded to approximately the present-day level at that time, prior to the opening of the Iapetus Ocean. Van den haute (1977) obtained fission track ages of ca. 240 Ma on apatites from the RIC, and postulated the former existence, of a thick sedimentary cover. In the Oslo graben (200 km to the NE), up to 1400 m of Lower Palaeozoic sediments have been preserved from erosion by the Permian downfaulting and to the west, while sediments of similar age have been involved in Caledonian nappe deformation. Therefore, the post-Sveconorwegian evolution can be sketched as follows: (1) uplift and erosion until ca. 600 Ma; (2) marine transgression and deposition of a thick sedimentary cover; (3) Caledonian metamorphism at ca. 400 Ma; (4) uplift and erosion of sedimentary cover, resumed erosion of the basement, related with Permian to Tertiary block faulting.

2.4. Fluid inclusions

Occurrence, composition and parageneses of fluid inclusions is related to the cooling and metamorphic evolution of the RIC. Their argon isotopic composition could have some importance on the interpretation of the $^{40}\text{Ar}/^{39}\text{Ar}$ data obtained on minerals, which carry fluid inclusions. Experiments on argon sorption carried out in quartz confirm that, in this mineral at least, a significant proportion of the argon released above 1000°C is associated with microinclusions ($< 1 \mu\text{m}$) (Roselieb et al., 1997). A study of fluid inclusions in charnockites from the Bjerkreim-Sokndal lapolith (Wilmart et al., 1991) can be to some point generalised to the whole of the RIC. Although mainly present in quartz, the inclusions also occur in other minerals. They rarely exceed 10–15 μm , some as small as 2 μm are still observable. Except for a few dense, pure CO_2 inclusions (Wilmart et al., 1991, 1994), which may represent the first fluid trapped at, or close, to magmatic conditions, all other inclusions (several types have been described) are associated with healed microcracks. For all CO_2 -bearing inclusions, the composi-

tional evolution is thought to correspond to that of a closed C–O–H system. The predominant graphite– CO_2 inclusions would have been trapped at about 600°C , under 3–4 kb, while some H_2O inclusions, at temperatures as high as 500°C . However, most of the late aqueous inclusions correspond to the introduction of external water, estimated to have occurred around 2–3 kb and 250°C . None exhibit NaCl-rich brines (halite cubes).

3. Experimental procedures

3.1. Sample preparation and characterisation

Eight plagioclases from different intrusions of the RIC (Fig. 1) were selected for $^{40}\text{Ar}/^{39}\text{Ar}$ analysis, with conventional stepwise-heating and UV-laser ablation. Three samples were from the cores of plagioclase megacrysts (up to 30 cm in length) that occur in the massif-type anorthosites (sample 84-18A from Egersund-Ogna, sample 92-16/7 from Hellenen and sample 72b/73 from Garsaknatt). For comparison, smaller (< 1 cm) plagioclase crystals have also been sampled in a banded layer in the Håland anorthosite–leuconorite (sample M88/7) and in the main leuconorite body of Garsaknatt (sample 56/73). The Hydra leuconoritic body has been investigated with some detail. Sample 0249-1/1 is a plagioclase concentrate separated from a medium grained (± 1.5 cm) leuconorite located at about 50 m from the contact with the (older) Farsund charnockite. Sample 0328-3/1 is the core of a megacryst (up to 20 cm in length), while sample 0065-1/5 is from a very coarse-grained (5 cm) anorthosite in the axial part of the massif.

After heavy liquid and magnetic separations, a high degree of purity of the plagioclase concentrate has been achieved by removal of all stained grains or impurities through hand-picking of the dry-sieved plagioclase fractions (180–500 μm) under binocular microscope ($40\times$ magnification). Macroscopically pure, undeformed, optically clear and transparent plagioclases were obtained; however, abundant minute impurities and/or inclusions and exsolutions are observed at high magnifications (Fig. 2A and B). Antiperthitic textures with rectangular blebs of K-

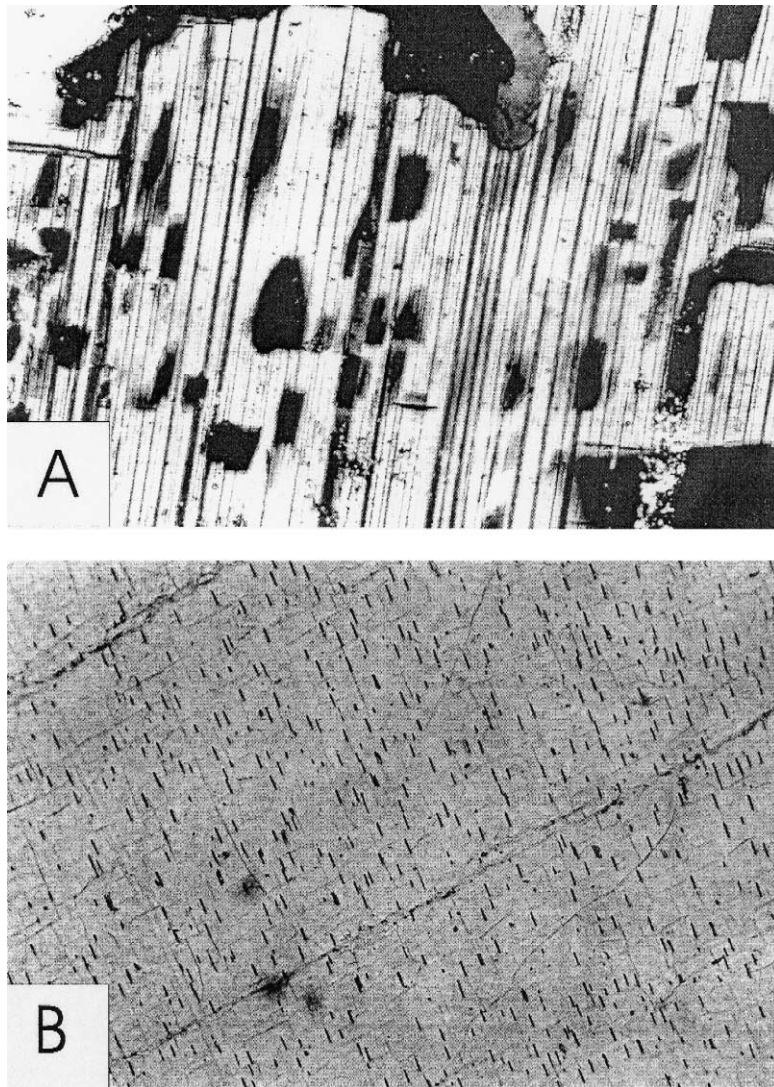


Fig. 2. (A) Photomicrograph of plagioclase 0065–1/5 from Hidra showing K-feldspar exsolution occurring as dark rectangular blebs (at a slight angle with the plagioclase twinning). Sericitisation occurs locally. Contains various types of mineral or fluid inclusions (magnification $\sim 150\times$). (B) Photomicrograph of abundant hemo-ilmenite needles within the same plagioclase sample (magnification $\sim 75\times$). Note also the microcracks and microcleavages filled with sericite (K-bearing phase).

feldspar and micromyrmekitic textures, such as described by Majer (1996) have been observed in restricted zones of the analysed plagioclases (Fig. 2A). Their temperature of formation corresponds to the “postmagmatic cooling stage” ($> 600^\circ\text{C}$) and partly to subsequent stages of regional cooling (Smith, 1984). Replacement antiperthites have not

been observed. Bøggild intergrowths producing macroscopically the typical blue irridescence, occur in two samples (0065-1/5 and 84-18A). Hemo-ilmenite platelets and needles (exsolution) are quite abundant, especially in the Hidra samples. They are distributed all over the megacrysts following two perpendicular orientations in the case of sample

0328-3/1. Their occurrence is related to the association between anorthosites and Fe–Ti-rich magmas (jotunites) (refer to Duchesne (1999) for an overview).

Some low temperature metamorphic minerals such as stilpnomelane, pumpellyite and prehnite have locally been observed within the plagioclases of the RIC (Sauter et al., 1983). The plagioclases are occasionally locally altered to kaolinite, sericite, laumontite and margarite. Sericite is generally only observed within very thin veins, which cross-cut the plagioclase megacrysts.

3.2. Stepwise-heating experiments

Two aliquots of each plagioclase sample were wrapped in high purity Al-foil and the foil capsules were stacked on top of each other within vacuum-sealed quartz-ampoules. Three ampoules (VUB-2, VUB-3, VUB-4) were irradiated under Cd-shielding at the BR-2 reactor of the Belgian Nuclear Research Centre SCK-CEN, in Mol. Each ampoule contained three aliquots of MMhb-1 hornblende age monitor (as supplied without further hand picking) and two aliquots of CaF_2 and K_2SO_4 salts to monitor the neutron fluence and the Ca and K argon isotope production rates, respectively. After half the projected irradiation time, each capsule was rotated, stacked in the same order and loaded at the same position in the channel, in order to compensate for the prevailing vertical gradient of the neutron flux. The gradient was also measured using 0.5 mm-thick Fe-wire placed parallel to each quartz-ampoule and cut into five equal pieces prior to a ^{54}Mn activity measurement. Each capsule received an average integrated fast neutron fluence (energy > 1 MeV) of 1.334 ± 0.007 , 1.287 ± 0.004 and 1.098 ± 0.009 in $10^{19} \text{ n cm}^{-2}$, respectively. Errors are stated at the 1 sigma level.

The activity measurements show that the fluence variation over the height of a capsule (55 mm) is less than 0.8%, corresponding with a high J -factor precision (for $J = 0.0841$ errors are < 0.0007). However, higher discrepancies ($\pm 5\%$) were measured among the J -factors obtained for the three unpurified aliquots of MMhb-1 placed in the same capsule. The

latter appears to be inhomogeneous, confirming previous reports by Baksi et al. (1996), Villa et al. (1996) and Renne et al. (1998) at the less than 15 mg aliquot level.

In the present study, an average J -value has been used for each ampoule and is referred to an age of 513.9 Ma for the primary standard MMhb-1 based on a cross-calibration with Fish Canyon sanidine results (Izett et al., 1992) and on K–Ar ages reported in Baksi et al. (1996). A more recent (Renne et al., 1998) age of 523.1 ± 4.6 Ma (based on intercalibration vs. GA-1550 as primary standard with an age of 98.79 ± 0.96 Ma) is more accurate, but the earlier calibration is retained here for comparison with the earlier work (Boven et al., 1996) and difference does not affect the conclusions, which are based upon the $^{40}\text{Ar}^*/^{39}\text{Ar}$ ratios. Ca/K ratios are deduced from the relative production rates for $^{37}\text{Ar}_{\text{Ca}}$ and $^{39}\text{Ar}_{\text{K}}$, whereby $\text{Ca}/\text{K} = 1.786 \times (^{37}\text{Ar}_{\text{Ca}}/^{39}\text{Ar}_{\text{K}})$. Correction factors for interfering argon isotopes produced by the neutron irradiation deduced from CaF_2 and K_2SO_4 salts irradiated together with the samples are $(^{36}\text{Ar}/^{37}\text{Ar})_{\text{Ca}} = 2.42 \times 10^{-4}$, $(^{39}\text{Ar}/^{37}\text{Ar})_{\text{Ca}} = 7.27 \times 10^{-4}$, $(^{38}\text{Ar}/^{39}\text{Ar})_{\text{K}} = 1.21 \times 10^{-2}$ and $(^{40}\text{Ar}/^{39}\text{Ar})_{\text{K}} = 9.23 \times 10^{-4}$, respectively. The two samples from Garsaknatt and the sample 0328-3/1 from Hydra were irradiated under the same conditions together with two aliquots of the biotite HD-B1 standard for which an age of 24.21 ± 0.32 Ma (Hess and Lippolt, 1994) was used. J -values are presented in Table 1.

Argon stepwise-heating analyses were carried out at the Vrije Universiteit Brussel $^{40}\text{Ar}/^{39}\text{Ar}$ laboratory on an MAP216 mass spectrometer operating in a static mode and equipped with a GS98 Bauer-Signer source, a Johnston electron multiplier and a manually retractable Faraday cup. Samples were incrementally heated in a high-vacuum resistance oven controlled by a Eurotherm controller and a thermocouple. Thermocouple readings as well as optical pyrometer measurements were used to obtain precise temperature calibration (better than $\pm 10^\circ\text{C}$) at different extraction furnace currents. Each sample underwent a similar sequential extraction–purification but with different temperature intervals between the steps. Oven temperatures were lowered to 250°C between each step. The whole volume of purified gases released during each step, or a known partition of this vol-

Table 1

A $^{40}\text{Ar}/^{39}\text{Ar}$ stepwise heating data on plagioclase separates

Temp (°C)	$^{40}\text{Ar}/^{39}\text{Ar}$	$^{37}\text{Ar}/^{39}\text{Ar}$	$^{36}\text{Ar}/^{39}\text{Ar}$ (10^{-3})	$^{38}\text{Ar}/^{39}\text{Ar}$ (10^{-3})	$^{37}\text{Ar}/^{38}\text{Ar}$	$^{40}\text{Ar}^*/^{37}\text{Ar}$	Ca/K	$^{40}\text{Ar}^*$ (%)	^{39}Ar Cum (%)	$^{40}\text{Ar}^*/^{39}\text{Ar}$	Apparent age ± 1 S.D. (in Ma)	1000/ T (1/K)	$-\log$ (D/r^2)
<i>Hidra sample 0065 1/5 aliquot (a), weight = 8.09 mg, VUB4: J = 0.0764</i>													
650	362.42	1.21	1138.13	234.68	5.15	21.60	2.16	7.20	5.76	26.10	1979 \pm 131	1.08	6.70
720	6.09	3.17	3.97	13.43	236.17	1.55	5.67	80.73	17.58	4.92	575 \pm 4	1.01	5.75
760	7.13	4.06	4.79	13.67	297.23	1.41	7.26	80.18	26.15	5.72	654 \pm 4	0.97	5.58
800	8.05	5.05	2.00	12.91	390.90	1.48	9.01	92.68	40.16	7.46	814 \pm 2	0.93	5.13
850	7.87	5.65	0.47	12.46	453.85	1.37	10.10	98.24	49.27	7.74	838 \pm 2	0.89	5.12
890	8.38	5.83	0.35	12.15	479.34	1.42	10.41	98.78	57.14	8.27	884 \pm 3	0.86	5.05
915	8.84	6.08	0.81	12.67	479.61	1.42	10.85	97.29	65.75	8.60	911 \pm 3	0.84	4.89
940	9.44	6.42	0.64	12.68	506.78	1.44	11.47	97.99	77.33	9.25	964 \pm 2	0.82	4.58
970	10.54	6.83	0.68	12.51	545.79	1.51	12.19	98.11	85.45	10.34	1050 \pm 3	0.80	4.54
1010	10.95	7.27	0.40	12.57	578.14	1.49	12.98	98.92	90.17	10.83	1088 \pm 3	0.78	4.58
1070	11.18	7.44	0.08	12.69	586.41	1.50	13.29	99.78	94.03	11.15	1112 \pm 6	0.74	4.47
1130	12.03	7.81	0.72	12.60	619.94	1.51	13.95	98.23	98.20	11.81	1160 \pm 4	0.71	4.09
1200	11.49	7.53	0.67	11.85	635.20	1.50	13.44	98.28	99.96	11.29	1122 \pm 13	0.68	3.87
1350	71.79	0.00	34.07	0.00	~	~	0.00	85.98	100.00	61.72	3145 \pm 132		
<i>Aliquot (b) weight = 6.48 mg, VUB4: J = 0.0764</i>													
650	133.50	1.50	408.99	89.17	16.84	8.42	2.68	9.47	5.20	12.64	1219 \pm 376	1.08	6.79
720	5.47	2.71	3.30	13.18	205.67	1.66	4.84	82.15	16.96	4.49	532 \pm 2	1.01	5.77
750	6.07	3.33	2.98	13.04	255.57	1.56	5.95	85.49	27.40	5.19	602 \pm 4	0.98	5.48
790	7.93	3.83	4.42	13.45	284.80	1.73	6.84	83.52	36.60	6.62	739 \pm 4	0.94	5.33
825	8.80	4.99	1.86	12.78	390.50	1.65	8.92	93.74	50.89	8.25	882 \pm 2	0.91	4.94
855	9.46	6.66	1.55	12.88	516.75	1.35	11.89	95.17	66.47	9.00	944 \pm 2	0.89	4.67
885	9.86	6.71	1.41	12.74	526.96	1.41	11.99	95.77	74.00	9.44	980 \pm 4	0.86	4.80
915	10.13	4.70	~	~	~	2.23	8.40	100.00	86.27	10.13	1034 \pm 87	0.84	4.38
935	12.91	7.76	3.26	13.33	582.17	1.54	13.86	92.55	90.03	11.95	1170 \pm 5	0.83	4.67
955	12.58	8.01	3.79	13.40	598.10	1.43	14.31	91.10	92.64	11.46	1135 \pm 10	0.81	4.69
1000	15.28	8.19	12.47	14.25	574.86	1.42	14.63	75.88	94.46	11.60	1145 \pm 15	0.79	4.72
1100	18.10	7.88	23.69	15.40	511.65	1.41	14.07	61.33	95.80	11.10	1108 \pm 15	0.73	4.73
1250	19.22	7.25	27.12	17.29	419.31	1.55	12.95	58.30	97.20	11.20	1116 \pm 14	0.66	4.56
1350	18.65	7.09	28.40	17.92	395.81	1.45	12.67	55.00	99.65	10.26	1044 \pm 12	0.62	3.85
1500	114.23	7.04	324.46	71.10	98.95	2.61	12.57	16.06	100.00	18.35	1581 \pm 60		
<i>Hidra sample 0249 1/1 aliquot (a), weight = 7.17 mg, VUB4: J = 0.0764</i>													
650	225.18	2.37	685.74	154.78	15.30	9.52	4.23	10.01	6.15	22.54	1807 \pm 196	1.08	6.64
720	9.10	2.30	6.43	15.85	145.36	3.13	4.12	79.12	19.10	7.20	791 \pm 2	1.01	5.67
760	8.73	2.21	6.94	14.85	148.98	3.02	3.95	76.52	28.72	6.68	744 \pm 3	0.97	5.48
800	8.16	2.58	2.49	13.65	189.37	2.87	4.62	90.98	38.57	7.43	811 \pm 3	0.93	5.27
840	11.78	3.19	2.07	13.35	238.97	3.50	5.70	94.81	49.89	11.17	1113 \pm 2	0.90	5.03
875	15.68	4.23	1.41	13.59	311.31	3.61	7.55	97.33	61.07	15.26	1394 \pm 3	0.87	4.87

900	17.32	4.39	1.01	13.58	322.96	3.88	7.84	98.28	68.66	17.02	1503 ± 3	0.85	4.89
925	17.91	4.46	0.63	13.51	330.27	3.97	7.97	98.96	75.66	17.72	1545 ± 2	0.83	4.80
950	18.61	4.55	0.60	13.23	343.95	4.05	8.13	99.05	82.70	18.44	1586 ± 3	0.82	4.65
975	23.20	5.91	0.46	13.50	437.79	3.90	10.56	99.41	87.06	23.07	1833 ± 4	0.80	4.72
1000	29.35	7.66	0.41	13.87	552.15	3.82	13.68	99.58	89.37	29.22	2117 ± 6	0.79	4.88
1035	34.71	9.25	0.73	13.43	688.48	3.73	16.52	99.38	91.64	34.50	2329 ± 4	0.76	4.79
1070	35.49	10.10	0.27	14.12	715.14	3.51	18.03	99.78	94.13	35.41	2363 ± 4	0.74	4.62
1110	36.46	9.68	~	13.76	703.48	3.77	17.29	100.00	97.12	36.46	2402 ± 4	0.72	4.32
1155	37.54	9.70	0.56	13.83	700.93	3.85	17.32	99.56	99.44	37.38	2435 ± 5	0.70	3.96
1210	35.49	7.86	~	12.02	654.12	4.52	14.04	100.00	99.89	35.49	2366 ± 19	0.67	4.26
1300	74.91	~	13.49	~	~	~	~	94.68	99.94	70.92	3354 ± 88	0.64	4.00
1450	117.80	~	123.59	18.01	~	~	~	69.00	99.98	81.28	3564 ± 103	0.58	4.00
1500	309.61	~	436.97	49.52	~	~	~	58.29	100.00	180.48	4860 ± 157		

Aliquot (b), weight = 8.07 mg, VUB4: J = 0.0764

550	115.38	3.43	282.92	97.17	35.25	9.27	6.12	27.54	1.50	31.77	2222 ± 56	1.21	7.88
600	98.51	2.35	256.94	69.96	33.56	9.62	4.19	22.92	3.69	22.58	1809 ± 18	1.15	7.17
690	210.27	5.05	571.63	187.42	26.95	8.19	9.02	19.67	6.15	41.36	2572 ± 29	1.04	6.83
720	7.35	2.41	1.36	9.66	249.51	2.88	4.30	94.53	14.33	6.94	768 ± 3	1.01	5.97
760	7.86	3.16	0.96	9.13	346.71	2.39	5.65	96.40	32.81	7.58	824 ± 2	0.97	5.20
790	9.54	3.36	1.13	8.39	400.36	2.74	6.00	96.51	42.72	9.21	961 ± 2	0.94	5.20
820	13.01	3.67	0.47	8.32	440.79	3.51	6.55	98.93	52.85	12.87	1235 ± 3	0.91	5.03
890	19.12	5.08	~	12.95	392.31	3.84	9.07	100.00	64.13	19.12	1624 ± 5	0.86	4.81
940	21.77	5.79	~	13.36	433.81	3.83	10.35	100.00	76.49	21.77	1767 ± 4	0.82	4.58
990	24.01	6.79	~	12.84	528.50	3.61	12.12	100.00	85.15	24.01	1879 ± 5	0.79	4.52
1050	32.03	7.94	~	12.50	635.39	4.11	14.18	100.00	90.23	32.03	2233 ± 8	0.76	4.55
1100	36.11	8.84	~	12.15	726.88	4.16	15.78	100.00	94.93	36.11	2389 ± 11	0.73	4.35
1160	34.94	9.28	~	11.67	794.92	3.84	16.57	100.00	98.74	34.94	2345 ± 13	0.70	4.03
1225	28.46	8.34	~	11.85	703.64	3.48	14.89	100.00	99.54	28.46	2084 ± 11	0.67	4.17
1400	25.14	3.51	~	13.14	267.37	6.26	6.28	87.54	100.00	22.01	1779 ± 22		

Hidra sample 0328-31, weight = 8.73 mg, VUB9: J = 0.09551

760	136.28	2.40	438.48	84.83	28.30	2.79	4.29	4.92	1.66	6.71	893 ± 104	0.97	7.79
800	7.72	6.25	2.01	~	~	1.14	11.16	92.32	3.35	7.12	936 ± 122	0.93	7.30
860	4.74	2.53	1.80	11.95	211.40	1.67	4.51	88.78	6.87	4.21	610 ± 2	0.88	6.66
900	4.62	3.09	1.41	11.81	261.78	1.36	5.52	90.97	10.86	4.20	609 ± 3	0.85	6.35
960	4.85	3.86	1.51	11.91	324.30	1.14	6.90	90.81	15.94	4.40	633 ± 3	0.81	6.05
1000	5.95	5.35	3.32	12.50	427.67	0.93	9.55	83.49	21.91	4.96	700 ± 5	0.79	5.81
1050	5.57	5.49	1.26	12.31	445.75	0.95	9.80	93.30	31.15	5.19	727 ± 4	0.76	5.44
1100	5.82	5.69	0.64	11.66	488.08	0.99	10.16	96.75	43.89	5.63	776 ± 14	0.73	5.09
1150	6.07	6.16	1.60	10.77	572.13	0.91	11.00	92.19	55.38	5.59	772 ± 32	0.70	4.94
1190	6.10	6.17	0.73	10.29	599.54	0.95	11.02	96.46	66.93	5.88	805 ± 16	0.68	4.76
1230	6.24	6.42	1.55	11.88	540.53	0.90	11.47	92.67	79.22	5.79	794 ± 19	0.67	4.53
1270	6.49	7.83	1.16	12.53	624.74	0.78	13.99	94.73	87.11	6.14	833 ± 3	0.65	4.50

(continued on next page)

Table 1 (continued)

Temp (°C)	⁴⁰ Ar/ ³⁹ Ar	³⁷ Ar/ ³⁹ Ar	³⁶ Ar/ ³⁹ Ar (10 ⁻³)	³⁸ Ar/ ³⁹ Ar (10 ⁻³)	³⁷ Ar/ ³⁸ Ar	⁴⁰ Ar* / ³⁷ Ar	Ca/K	⁴⁰ Ar* (%)	³⁹ Ar Cum (%)	⁴⁰ Ar* / ³⁹ Ar	Apparent age ± 1 S.D. (in Ma)	1000/T (1/K)	- log (D/r ²)
<i>Hidra sample 0328-31, weight = 8.73 mg, VUB9: J = 0.09551</i>													
1300	6.66	7.99	1.79	12.96	616.70	0.77	14.28	92.07	92.07	6.13	831 ± 6	0.64	4.48
1340	7.72	8.27	4.21	13.13	629.94	0.78	14.77	83.90	93.15	6.48	869 ± 4	0.62	5.00
1410	7.79	7.79	4.37	13.43	580.13	0.83	13.92	83.43	95.53	6.50	871 ± 2	0.59	4.54
1570	7.39	7.43	3.24	12.63	588.00	0.87	13.27	87.05	99.16	6.44	865 ± 2	0.54	3.95
1700	29.02	8.19	74.98	27.92	293.17	0.84	14.62	23.64	100.00	6.86	909 ± 14		
<i>Garsaknatt sample 56 / 73, weight = 15.54 mg, VUB9: J = 0.09551</i>													
760	81.06	2.80	258.66	48.44	57.77	1.65	5.00	5.71	3.65	4.63	661 ± 77	0.97	7.10
800	4.77	3.22	4.00	7.99	403.07	1.11	5.75	75.21	5.30	3.59	532 ± 17	0.93	7.05
860	5.22	3.07	6.77	10.04	305.60	1.05	5.48	61.67	7.16	3.22	484 ± 10	0.88	6.85
900	4.19	3.15	2.12	7.62	413.10	1.13	5.62	85.01	10.98	3.56	528 ± 5	0.85	6.36
980	2.95	3.19	1.22	7.12	448.84	0.81	5.71	87.80	19.69	2.59	399 ± 2	0.80	5.75
1000	2.94	3.46	0.39	11.37	304.69	0.82	6.19	96.13	35.87	2.83	432 ± 11	0.79	5.17
1050	3.05	3.32	0.22	11.17	297.37	0.90	5.93	97.82	51.71	2.99	453 ± 6	0.76	4.89
1290	3.32	3.83	0.26	11.54	331.94	0.85	6.84	97.64	68.41	3.24	487 ± 4	0.64	4.62
1410	4.01	4.27	0.32	11.39	374.55	0.92	7.62	97.67	83.16	3.92	573 ± 11	0.59	4.39
1465	33.95	5.03	92.25	30.97	162.54	1.33	8.99	19.70	89.90	6.69	891 ± 18	0.58	4.47
1570	46.39	5.03	131.49	38.47	130.77	1.50	8.99	16.24	98.36	7.53	978 ± 14	0.54	3.91
1700	97.91	4.07	298.76	78.56	51.84	2.36	7.27	9.83	100.00	9.62	1176 ± 63		
<i>Garsaknatt sample 72b / 73, weight = 12.33 mg, VUB9: J = 0.09551</i>													
880	44.24	1.11	135.21	36.99	30.02	3.86	1.98	9.69	7.79	4.28	619 ± 16	0.87	6.43
930	3.83	1.32	1.18	11.28	117.48	2.62	2.37	90.88	12.61	3.48	517 ± 26	0.83	6.21
980	3.90	2.14	1.09	11.79	181.46	1.67	3.82	91.72	20.94	3.58	531 ± 2	0.80	5.72
1000	4.15	2.72	0.82	11.81	230.58	1.44	4.86	94.14	28.50	3.91	572 ± 2	0.79	5.57
1030	4.66	3.45	0.99	11.91	290.08	1.26	6.17	93.70	31.96	4.36	628 ± 4	0.77	5.79
1050	16.47	3.59	38.39	19.46	184.43	1.43	6.41	31.11	36.25	5.12	719 ± 20	0.76	5.63
1080	6.96	4.23	6.14	13.16	321.53	1.22	7.56	73.95	41.19	5.15	721 ± 3	0.74	5.49
1100	6.27	4.69	2.27	12.32	380.94	1.19	8.38	89.30	48.32	5.59	772 ± 3	0.73	5.23
1130	5.77	5.00	0.54	12.36	404.57	1.12	8.93	97.25	52.33	5.61	774 ± 4	0.71	5.39
1150	5.83	5.25	0.54	12.15	432.04	1.08	9.37	97.29	56.85	5.67	781 ± 3	0.70	5.28
1170	6.11	5.50	1.14	12.05	456.66	1.05	9.83	94.47	62.22	5.78	793 ± 3	0.69	5.12
1190	6.26	5.62	1.07	12.13	463.66	1.06	10.05	94.96	66.99	5.94	811 ± 4	0.68	5.09
1230	6.50	5.59	1.64	12.44	449.59	1.08	9.99	92.55	71.31	6.02	819 ± 4	0.67	5.06
1250	6.29	5.48	1.02	12.23	448.24	1.09	9.79	95.22	76.25	5.98	816 ± 3	0.66	4.92
1270	6.24	5.45	0.74	12.20	447.00	1.11	9.74	96.51	82.05	6.03	820 ± 3	0.65	4.74
1300	6.60	5.92	1.57	12.42	476.93	1.04	10.58	92.96	85.11	6.14	832 ± 5	0.64	4.91
1320	6.74	6.20	0.92	12.15	509.98	1.04	11.07	95.94	87.98	6.46	867 ± 5	0.63	4.84
1375	6.99	6.66	1.87	12.40	537.04	0.97	11.89	92.11	90.96	6.44	865 ± 4	0.61	4.72
1450	6.71	6.43	1.11	12.25	525.29	0.99	11.49	95.14	94.77	6.39	859 ± 4	0.58	4.43

1570	6.94	6.53	1.99	12.30	530.80	0.97	11.66	91.53	98.96	6.35	855 ± 4	0.54	3.96
1700	18.37	8.14	37.49	19.24	422.82	0.90	14.53	39.69	100.00	7.29	953 ± 13		
<i>Egersund-Ogna sample 84-18A, weight = 5.30 mg VUB3: J = 0.0841</i>													
750	7.65	~	15.01	14.67	~	~	~	42.06	17.95	3.22	432 ± 45	0.98	5.68
800	5.48	7.77	4.35	17.57	442.52	0.54	13.88	76.55	26.82	4.20	545 ± 10	0.93	5.55
875	5.44	11.48	1.44	13.61	843.11	0.44	20.50	92.19	40.71	5.01	635 ± 5	0.87	5.12
950	6.26	12.88	1.08	13.66	942.83	0.46	23.01	94.92	54.66	5.94	731 ± 5	0.82	4.89
1048	6.48	13.44	1.14	13.43	1000.93	0.46	24.01	94.82	68.36	6.15	752 ± 5	0.76	4.68
1141	6.33	13.37	0.76	12.87	1039.21	0.46	23.88	96.44	91.93	6.11	748 ± 3	0.71	4.05
1200	6.64	13.17	0.64	12.74	1033.42	0.49	23.51	97.14	100.00	6.45	782 ± 8		
<i>Haland sample M88 / 7 aliquot (a), weight = 5.42 mg, VUB4: J = 0.0764</i>													
710	347.83	1.30	1116.32	231.37	5.61	13.83	2.32	5.16	2.90	17.96	1558 ± 432	1.02	7.30
750	5.72	1.98	5.91	13.47	146.67	2.01	3.53	69.47	8.50	3.97	478 ± 5	0.98	6.41
790	5.11	2.66	3.43	13.17	201.81	1.54	4.75	80.14	12.07	4.09	491 ± 7	0.94	6.33
830	4.90	2.80	2.36	12.60	222.10	1.50	5.00	85.75	18.06	4.20	502 ± 4	0.91	5.92
860	5.14	3.14	2.16	12.59	249.09	1.43	5.60	87.59	24.30	4.50	533 ± 4	0.88	5.73
910	5.30	3.25	1.62	12.62	257.33	1.48	5.80	90.95	29.85	4.82	565 ± 5	0.85	5.65
960	5.35	3.36	0.94	12.83	262.21	1.51	6.01	94.79	36.41	5.07	590 ± 4	0.81	5.46
1000	5.84	3.25	0.73	12.96	250.78	1.73	5.80	96.30	58.75	5.62	645 ± 2	0.79	4.68
1045	6.91	4.71	0.69	13.04	360.96	1.43	8.41	97.06	66.73	6.71	747 ± 2	0.76	4.90
1090	7.10	5.33	0.69	12.99	410.02	1.30	9.51	97.15	76.25	6.90	764 ± 2	0.73	4.67
1150	7.08	5.44	0.56	12.76	426.27	1.27	9.72	97.68	88.57	6.92	765 ± 2	0.70	4.31
1230	6.84	4.71	0.79	12.85	366.14	1.40	8.40	96.58	99.89	6.60	737 ± 2	0.67	3.59
1350	41.92	2.25	63.23	21.68	103.75	10.33	4.02	55.42	100.00	23.23	1841 ± 111		
<i>Aliquot (b) weight = 6.99 mg, VUB4: J = 0.0764</i>													
650	428.07	1.43	1409.28	275.80	5.17	8.15	2.55	2.72	2.20	11.62	1147 ± 579	1.08	7.55
720	6.97	1.71	7.45	13.80	123.86	2.79	3.05	68.40	5.17	4.77	560 ± 14	1.01	6.88
760	5.86	2.74	4.13	13.03	210.39	1.69	4.90	79.20	8.68	4.64	548 ± 8	0.97	6.52
800	5.39	3.10	2.81	12.53	247.80	1.47	5.54	84.59	13.93	4.56	539 ± 5	0.93	6.12
840	5.57	3.47	2.39	12.48	278.27	1.40	6.20	87.30	20.58	4.86	570 ± 6	0.90	5.81
880	5.97	3.91	1.86	12.71	307.85	1.39	6.99	90.79	25.90	5.42	625 ± 7	0.87	5.75
925	5.85	4.23	0.75	12.53	337.25	1.33	7.55	96.23	35.94	5.63	645 ± 4	0.83	5.32
1000	6.14	4.10	0.78	12.73	322.31	1.44	7.33	96.25	50.18	5.91	673 ± 3	0.79	4.95
1050	6.64	4.57	0.51	12.90	354.05	1.42	8.16	97.71	62.29	6.49	727 ± 3	0.76	4.82
1110	7.11	5.15	0.35	12.78	403.05	1.36	9.20	98.53	69.30	7.01	774 ± 5	0.72	4.91
1180	7.36	5.49	0.22	13.01	422.25	1.33	9.81	99.13	74.14	7.30	799 ± 5	0.69	4.97
1240	7.42	5.89	0.36	12.90	456.83	1.24	10.52	98.56	81.46	7.31	800 ± 5	0.66	4.66
1350	7.11	5.62	0.44	12.65	444.43	1.24	10.04	98.19	97.58	6.98	771 ± 2	0.62	3.86
1450	12.03	4.59	0.48	11.38	403.18	2.59	8.20	98.81	98.17	11.89	1166 ± 48	0.58	4.72
1550	10.91	4.94	4.81	13.14	376.30	1.92	8.83	86.96	99.26	9.48	983 ± 20	0.55	4.21
1750	14.36	4.89	12.67	15.41	317.51	2.17	8.74	73.93	100.00	10.62	1071 ± 40		

(continued on next page)

Table 1 (continued)

Temp (°C)	$^{40}\text{Ar}/^{39}\text{Ar}$	$^{37}\text{Ar}/^{39}\text{Ar}$	$^{36}\text{Ar}/^{39}\text{Ar}$ (10^{-3})	$^{38}\text{Ar}/^{39}\text{Ar}$ (10^{-3})	$^{37}\text{Ar}/^{38}\text{Ar}$	$^{40}\text{Ar}^*/^{37}\text{Ar}$	Ca/K	$^{40}\text{Ar}^*$ (%)	^{39}Ar Cum (%)	$^{40}\text{Ar}^*/^{39}\text{Ar}$	Apparent age ± 1 S.D. (in Ma)	$1000/T$ (1/K)	$-\log$ (D/r^2)
<i>Helleren sample 92 16/7, weight = 6.19 mg, VUB3: J = 0.0841</i>													
650	24.02	2.00	55.15	25.96	77.00	3.86	3.57	32.16	3.51	7.73	903 ± 504	1.08	7.14
700	5.89	1.49	4.32	13.11	113.71	3.09	2.66	78.33	7.68	4.61	591 ± 6	1.03	6.55
750	5.80	2.38	4.00	13.54	176.07	1.94	4.26	79.63	13.73	4.62	592 ± 4	0.98	6.08
790	6.13	3.33	3.45	13.26	251.43	1.53	5.95	83.37	20.87	5.11	645 ± 3	0.94	5.78
820	6.57	4.24	2.67	13.26	319.89	1.36	7.57	87.96	26.87	5.78	714 ± 4	0.91	5.68
860	6.46	4.45	1.56	13.57	328.29	1.35	7.96	92.87	35.72	6.00	737 ± 3	0.88	5.36
895	7.03	4.74	0.97	12.59	376.17	1.42	8.46	95.90	45.69	6.74	811 ± 3	0.86	5.15
955	7.31	4.71	0.64	12.62	373.24	1.51	8.41	97.39	54.81	7.12	846 ± 2	0.81	5.04
925	7.21	4.49	0.72	12.45	360.48	1.56	8.02	97.07	65.65	6.99	835 ± 2	0.83	4.80
990	7.60	5.08	0.55	12.35	411.00	1.47	9.07	97.87	70.53	7.44	877 ± 3	0.79	5.03
1060	7.76	5.25	0.52	12.38	423.84	1.45	9.37	98.02	74.78	7.60	892 ± 4	0.75	5.00
1150	7.69	5.83	0.67	12.55	464.86	1.29	10.42	97.41	82.58	7.50	882 ± 2	0.70	4.62
1240	7.54	5.77	0.57	12.37	466.13	1.28	10.30	97.77	95.28	7.37	870 ± 2	0.66	4.06
1350	7.97	5.48	1.05	12.42	441.08	1.40	9.79	96.10	98.93	7.65	897 ± 6	0.62	4.00
1450	22.98	3.05	26.60	16.73	182.12	4.96	5.44	65.80	99.13	15.12	1480 ± 54	0.58	4.85
1500	25.22	3.12	34.91	18.19	171.71	4.77	5.58	59.10	99.34	14.91	1466 ± 72	0.56	4.73
1550	21.41	3.55	34.87	16.70	212.78	3.13	6.35	51.87	99.70	11.11	1190 ± 49	0.55	4.27
1600	32.73	3.06	58.41	19.19	159.22	5.06	5.46	47.27	99.90	15.47	1503 ± 53	0.53	4.89
1700	56.67	0.96	112.76	23.05	41.80	24.24	1.72	41.20	100.00	23.35	1960 ± 86		

Isotopic ratios are corrected for mass discrimination, blank line levels, atmospheric contamination, and flux gradients. The quoted error on ages is one standard deviation. The J values are calculated as the average of the 513.9 Ma age of MMhb-1 and $24.21 \pm \text{Ma}$ HD-B1 standards in each vial. Last two columns show the $\log D/r^2$ and $1000/T$ (K) values calculated after MDD program from Lovera et al. (1989).

Table 2
Plagioclase UV laser ablation data on thick sections

Sample nature	Spot #	Crater size (μm)	^{40}Ar (mV)	$^{40}\text{Ar}/^{36}\text{Ar}$	$^{40}\text{Ar}/^{39}\text{Ar}$	$^{37}\text{Ar}/^{39}\text{Ar}$	$^{37}\text{Ar}/^{38}\text{Ar}$	$^{40}\text{Ar}^*/^{39}\text{Ar}$	Ca/K	Apparent age ± 1 S.D. (Ma)
<i>Hidra sample 0065-1 / 5 (J = 0.005296)</i>										
P	27	50 × 50	16.45	449.92	127.16	13.46	~	43.64	24.04	375 ± 107
P	1	50 × 50	43.48	923.18	80.86	12.04	~	54.98	21.50	461 ± 77
P	2	50 × 50	145.87	670.65	110.52	3.68	346.92	61.83	6.57	511 ± 25
P	3	50 × 50	44.80	948.92	94.04	12.66	~	64.76	22.60	532 ± 63
P	32	50 × 50	26.40	996.78	93.20	7.07	218.50	65.57	12.62	538 ± 67
P	4	50 × 50	46.00	977.43	96.65	13.88	~	67.43	24.79	551 ± 50
P	5	50 × 50	27.08	~	72.18	7.54	~	72.75	13.47	588 ± 44
MI	20	50 × 50	21.55	3296.41	88.94	7.47	93.53	80.97	13.34	644 ± 56
FI	22	50 × 50	26.91	~	82.95	6.21	~	83.42	11.09	660 ± 50
P	6	50 × 50	53.00	935.02	125.12	19.09	181.46	85.58	34.08	674 ± 68
MI	12	50 × 50	28.55	1730.43	104.56	7.19	214.22	86.70	12.84	682 ± 94
P	7	50 × 50	10.29	605.41	175.71	0.00	~	89.94	0.00	703 ± 232
FI	21	50 × 50	19.61	~	92.92	12.22	~	93.84	21.82	728 ± 62
P	8	50 × 50	49.38	~	93.43	9.22	~	94.12	16.46	730 ± 47
P	31	50 × 50	12.20	~	94.17	11.43	161.45	95.03	20.40	735 ± 130
P	9	50 × 50	46.31	~	94.97	9.23	321.50	95.66	16.49	739 ± 61
P	10	50 × 50	34.94	~	98.45	6.98	~	98.98	12.47	760 ± 48
P	11	50 × 50	33.47	~	103.39	9.21	325.20	104.08	16.44	792 ± 54
MI	13	50 × 50	21.18	~	105.17	7.71	~	105.76	13.77	802 ± 113
MI	19	50 × 50	31.58	~	107.81	10.38	~	108.59	18.54	820 ± 61
P	26	50 × 50	26.42	995.88	155.07	10.83	201.38	109.05	19.35	822 ± 104
MI	14	100 × 10	68.82	591.85	219.46	9.02	308.75	109.89	16.11	827 ± 57
FI + V	17	50 × 50	20.05	~	110.80	7.45	69.68	111.36	13.30	836 ± 99
MI	18	50 × 50	24.62	~	111.28	11.65	281.34	112.16	20.81	841 ± 105
P	33	50 × 50	26.43	~	114.08	10.45	~	114.87	18.66	857 ± 77
FI	23	50 × 50	24.98	~	124.44	12.85	~	125.41	22.94	919 ± 67
P	28	50 × 50	59.60	~	129.99	2.89	44.79	130.21	5.15	946 ± 69
P	25	50 × 50	47.16	~	132.83	6.54	120.02	133.32	11.68	964 ± 76
MI	24	50 × 50	131.56	1364.81	184.09	3.32	258.97	144.23	5.93	1024 ± 37
FI	16	50 × 50	62.10	1699.08	245.81	6.96	~	203.06	12.43	1317 ± 86
P + FI	34	50 × 50	244.60	1659.44	296.03	6.40	377.75	243.32	11.43	1494 ± 88
FI	15	50 × 50	143.58	8806.99	353.53	6.73	298.12	341.67	12.01	1864 ± 90
P + FI	29	50 × 50	170.49	4656.93	805.35	7.24	~	754.25	12.92	2902 ± 150
P	30	50 × 50	16.79	193.94	120.22	12.09	184.27	~	21.60	~
<i>Hidra sample 0249-1 / 1 (J = 0.005296)</i>										
CP	35	50 × 50	29.48	337.53	76.73	14.38	228.48	9.55	25.68	89 ± 61
P	36	100 × 100	90.17	483.29	94.15	8.90	~	36.58	15.90	320 ± 24
P	37	50 × 50	77.56	525.43	100.02	5.75	184.41	43.77	10.27	376 ± 34
P	38	50 × 50	104.64	559.07	115.26	6.86	53.76	54.34	12.25	456 ± 29
P	39	50 × 50	101.68	691.09	126.31	7.92	34.06	72.30	14.14	585 ± 40
P	40	50 × 50	58.98	2159.70	90.55	8.68	~	78.16	15.51	625 ± 37
P + MI	41	50 × 50	60.45	2227.96	95.90	10.07	453.08	83.18	17.97	659 ± 45
CP + MI	42	50 × 50	34.45	~	84.85	9.24	155.06	85.54	16.50	674 ± 60
CP	43	50 × 50	62.57	~	87.41	7.45	28.56	87.97	13.30	690 ± 28
CP + MI	44	50 × 50	106.48	3859.31	95.54	4.08	~	88.23	7.28	692 ± 39
CP	45	50 × 50	127.63	2683.75	134.35	4.92	104.99	119.56	8.79	885 ± 47
P	46	50 × 50	133.82	1334.75	153.60	3.83	31.73	119.59	6.84	885 ± 43
P	47	50 × 50	107.21	13630.80	134.58	4.35	247.70	131.66	7.77	954 ± 27
P	48	100 × 100	268.93	3493.72	145.96	3.78	127.12	133.61	6.74	965 ± 19

(continued on next page)

Table 2 (continued)

Sample nature	Spot #	Crater size (μm)	^{40}Ar (mV)	$^{40}\text{Ar}/^{36}\text{Ar}$	$^{40}\text{Ar}/^{39}\text{Ar}$	$^{37}\text{Ar}/^{39}\text{Ar}$	$^{37}\text{Ar}/^{38}\text{Ar}$	$^{40}\text{Ar}^*/^{39}\text{Ar}$	Ca/K	Apparent age ± 1 S.D. (Ma)
<i>Hidra sample 0249-1 / 1 (J = 0.005296)</i>										
CP + MI	49	50 \times 50	91.79	~	160.62	10.45	~	161.41	18.66	1115 \pm 63
CP + MI	50	50 \times 50	502.37	1402.84	260.61	1.30	29.40	205.71	2.32	1329 \pm 13
CP + MI	51	50 \times 50	130.02	2261.12	236.79	8.93	202.60	205.85	15.94	1330 \pm 44
CP	52	100 \times 100	503.28	3979.21	317.67	5.63	137.27	294.08	10.05	1694 \pm 36
MI	54	50 \times 50	247.13	6696.26	582.60	17.05	111.38	556.89	30.44	2478 \pm 101
MI	55	50 \times 50	184.66	1361.49	3628.32	240.32	505.68	2840.82	429.15	5007 \pm 449
MI	56	50 \times 50	218.78	1061.38	5218.03	245.06	97.25	3765.28	437.61	5488 \pm 899
MI	57	50 \times 50	266.02	1808.62	19543.34	479.35	146.44	16350.26	855.97	8069 \pm 1764
MI	53	50 \times 50	543.20	8201.15	~	~	151.92	~	~	~
<i>Hidra sample 0328-3 / 1 (J = 0.005296)</i>										
CP	60	100 \times 100	111.61	825.65	95.08	6.08	241.83	61.05	10.86	505 \pm 23
MI	61	50 \times 50	213.31	~	61.91	1.89	130.41	62.05	3.37	513 \pm 8
CP	58	100 \times 100	108.42	1438.44	80.98	4.77	160.65	64.34	8.51	529 \pm 23
CP	59	100 \times 100	128.29	1217.68	92.97	4.66	332.56	70.41	8.33	572 \pm 14
MI	62	50 \times 50	50.49	~	77.54	7.78	~	78.12	13.89	625 \pm 31
<i>Garsaknatt sample 72b / 73 (J = 0.005296)</i>										
MI	78	50 \times 50	51.15	351.05	88.30	8.77	~	13.97	15.67	129 \pm 27
P	63	200 \times 15	44.87	588.72	100.38	6.84	~	50.00	12.21	424 \pm 38
MI	77	200 \times 15	94.50	697.07	92.58	5.50	~	53.33	9.83	449 \pm 21
P	64	220 \times 15	66.42	693.00	95.89	6.57	75.71	55.00	11.73	461 \pm 31
MI	76	100 \times 100	184.62	820.52	91.57	3.89	157.29	58.59	6.95	488 \pm 15
P	65	50 \times 50	41.13	732.14	101.36	7.92	166.20	60.45	14.15	501 \pm 46
MI	75	50 \times 50	107.71	1638.30	79.78	3.64	~	65.39	6.50	536 \pm 20
MI	74	200 \times 15	45.02	2853.91	75.03	8.01	248.23	67.27	14.30	550 \pm 27
P + MI	73	50 \times 50	251.56	3825.49	72.99	1.41	69.29	67.35	2.52	550 \pm 10
P	66	220 \times 15	149.84	1751.45	99.65	3.77	~	82.84	6.73	656 \pm 14
MI	72	320 \times 10	95.09	2083.72	99.13	5.57	~	85.07	9.95	671 \pm 26
P	67	100 \times 100	152.65	10033.48	87.77	4.03	237.10	85.19	7.19	672 \pm 15
P	68	50 \times 50	73.31	2043.64	99.90	6.03	~	85.45	10.76	674 \pm 35
P	69	50 \times 50	82.58	1096.84	117.72	9.56	731.75	86.01	17.07	677 \pm 37
P + MI	71	200 \times 10	29.48	~	108.01	7.68	~	108.59	13.71	820 \pm 84
P + MI	70	50 \times 50	139.49	1028.22	187.60	7.05	~	133.68	12.59	966 \pm 43
<i>Egersund-Ogna sample 84-18A (J = 0.005296)</i>										
P + MI	85	50 \times 50	14.38	385.12	85.39	32.62	~	19.87	58.25	181 \pm 132
P + MI	84	50 \times 50	16.16	593.18	102.34	37.54	~	51.36	67.03	434 \pm 144
P	81	50 \times 50	18.61	~	63.61	14.85	~	64.73	26.52	532 \pm 71
P	79	50 \times 50	56.98	983.43	105.53	5.88	131.28	73.82	10.50	595 \pm 51
P	80	50 \times 50	30.92	4125.85	90.02	14.33	~	83.57	25.58	661 \pm 70
P	82	50 \times 50	34.43	4527.12	89.44	11.67	~	83.60	20.84	661 \pm 63
P + MI	86	100 \times 100	49.93	~	89.75	16.90	~	91.02	30.18	710 \pm 46
FI	87	50 \times 50	45.66	6033.75	104.68	10.63	1213.79	99.56	18.98	764 \pm 69
P	83	50 \times 50	63.29	1355.63	161.13	20.59	334.32	126.01	36.76	922 \pm 84
<i>Helleren sample 92-16 / 7 (J = 0.005296)</i>										
P + V	94	50 \times 50	~	921.44	68.43	7.12	~	46.48	12.71	397 \pm 47
MI + V	95	50 \times 50	46.78	704.48	85.01	4.29	~	49.35	7.67	419 \pm 42
P + MI	97	50 \times 50	30.48	654.57	96.96	5.48	58.33	53.19	9.79	448 \pm 55
MI + V	96	50 \times 50	37.10	654.83	98.61	3.59	~	54.11	6.40	455 \pm 47
P + MI	93	50 \times 50	49.52	1362.62	85.24	4.43	~	66.76	7.92	546 \pm 27
P	90	50 \times 50	28.00	1049.65	95.21	4.32	43.02	68.41	7.72	558 \pm 53

Table 2 (continued)

Sample nature	Spot #	Crater size (μm)	^{40}Ar (mV)	$^{40}\text{Ar}/^{36}\text{Ar}$	$^{40}\text{Ar}/^{39}\text{Ar}$	$^{37}\text{Ar}/^{39}\text{Ar}$	$^{37}\text{Ar}/^{38}\text{Ar}$	$^{40}\text{Ar}^*/^{39}\text{Ar}$	Ca/K	Apparent age ± 1 S.D. (Ma)
<i>Helleren sample 92-16/7 ($J = 0.005296$)</i>										
P + MI	92	50 \times 50	57.85	873.73	105.23	5.64	160.25	69.64	10.07	566 \pm 25
P	91	100 \times 100	125.17	1086.52	98.04	5.53	364.65	71.37	9.87	578 \pm 26
P	88	50 \times 50	32.52	1981.71	94.32	6.72	119.71	80.26	12.00	639 \pm 72
P	89	100 \times 100	126.07	~	88.17	5.90	921.10	88.61	10.54	694 \pm 19
V	98	200 \times 20	60.55	9841.62	100.75	5.53	362.50	97.73	9.87	753 \pm 29

P = clear plagioclase; CP = cloudy plagioclase; MI = mineral inclusion; FI = surmised fluid inclusion; V = microvein; ~ = too small ^{36}Ar and/or ^{38}Ar peak.

ume, were measured with either the Faraday cup or the multiplier (depending on the intensity of the signal). The multiplier gain and mass discrimination have been checked regularly through measurement on a partition of an air pipette.

The complete $^{40}\text{Ar}/^{39}\text{Ar}$ data set is presented in Table 1. Argon isotopic results include dynamic background, mass discrimination and K and Ca interference corrections. They do not include the 0.8% error estimate on the J -factor known from the dosimetry measurement, the unknown interlaboratory error on the J -factor because of variations in the reported K–Ar age of standards and the errors on the K, Ca correction factors. This approach is relevant since particular attention is drawn on the interstep comparison of the argon isotope composition. Inter-sample reproducibility can be estimated on the basis of the duplicate measurements.

3.3. UV-laser ablation experiments

In addition to samples prepared for stepwise heating, one-side polished, ca. 120 μm -thick sections were prepared for UV-laser ablation $^{40}\text{Ar}/^{39}\text{Ar}$ analyses. This technique was used for the Hydra, Helleren and Egersund-Ogna samples and for one sample from Garsaknatt (72b/73). Thick sections were irradiated without Cd shielding at the RISO3 reactor in Denmark together with the biotite flux monitor GA1550 (98.79 ± 0.96 Ma; Renne et al., 1998). Correction factors are $(^{36}\text{Ar}/^{37}\text{Ar})_{\text{Ca}} = 2.55 \times 10^{-4}$, $(^{39}\text{Ar}/^{37}\text{Ar})_{\text{Ca}} = 0.67 \times 10^{-3}$ and $(^{40}\text{Ar}/^{39}\text{Ar})_{\text{K}} = 4.8$

$\times 10^{-2}$, respectively. The J -value reported in Table 2 is the average of seven out of eight IR-laser single or double grain total fusion analyses. The UV-laser analyses were carried out on a MAP215-50 mass spectrometer and a Spectron 401 quadrupled Nd-YAG ($\lambda = 266$ nm) laser, using the experimental setup described in Arnaud and Kelley (1995). Different modifications of the ablation procedure were adopted during the present experiment. The laser beam was slightly defocused during the rastering of 50 \times 50 or 100 \times 100 μm squared pits within homogeneous parts of the plagioclase, increasing the amounts of sample ablated. This resulted in a release of up to twice as much Ar for equivalent rastering times and only slightly diffuse margins of the ablation crater. Ablation along rectangular tracks allowed ablation of the elongated hemo-ilmenite inclusions. A similar type of rastering was performed in order to ablate elongated pits parallel to the orientation of plagioclase lamellae. This procedure is expected to detect lamellae dependent Ar-isotopic or K heterogeneity.

3.4. Electron microprobe analysis

Two sets of electron microprobe analyses were performed to detect compositional changes within the plagioclases. In a first set of experiments scanning profiles were obtained on small cleavage fragments of an $^{40}\text{Ar}/^{39}\text{Ar}$ aliquot (totally free of any sign of cloudiness) from the core of the megacrysts of Egersund-Ogna (sample 84-18A) and Hydra (sam-

ple 0065-1/5) in order to evaluate sample homogeneity. An additional set of measurements was obtained on unirradiated polished sections of the same samples on which UV-laser ablation experiments were performed.

For the first set of analyses, a CAMEBAX-SX-50 electron microprobe (CAMST, Université Catholique de Louvain, Belgium) equipped with 4 WDS spectrometers and two or four monochromators has been operated with an accelerating voltage of 15 kV and a beam current of 20 μ A. All data were corrected using ZAF procedures. The second set of analyses were performed on a CAMECA-SX-100 electron microprobe (Open University, UK) equipped with 4 WDS spectrometers and operated with an accelerating voltage of 20 kV and a beam current of 20 μ A.

4. Results

4.1. Stepwise heating

The argon-release spectra for each sample are presented in Fig. 3 together with the variation of the Ca/K (deduced from the $^{37}\text{Ar}_{\text{Ca}}/^{39}\text{Ar}_{\text{K}}$) and plots of Ca/K vs. $^{40}\text{Ar}^*/^{39}\text{Ar}$ ratios. The overall pattern of these spectra has generally been termed “saddle-shaped” (Dalrymple and Lanphere, 1974). They exhibit similar features: an initially high set of ages (developed in some but not all samples), followed by a low and then a staircase rise, sometimes up to a pseudo-plateau, sometimes until fusion. The relative importance of these features varies, however, between samples.

In detail, plagioclase separates 0065-1/5 and 0249-1/1 from the Hydra massif (south of the area) exhibit reproducible patterns even when run as two aliquots. Both exhibit initial ages older than the U/Pb intrusion age (930 Ma) followed by ages of 532 to 575 Ma (sample 0065-1/5) and 768 to 791 Ma (sample 0249-1/1), then ages rise to around 1100 Ma for sample 0065-1/5 and close to 2500 Ma for sample 0249-1/1. The latter apparent ages are much greater than the plausible intrusion age and are, therefore, attributed to the presence of excess

argon. However, the third sample 0328-3/1 from the Hydra massif, corresponding to the core of a megacryst (< 30 cm) exhibits lower ages: initially high ages in the range 893–936 Ma fall to 610 Ma, followed by a staircase rise, a subplateau around 775 Ma and, finally, rising to around 870 Ma. Although there is no true plateau, these higher ages are in the range expected for post-Sveconorwegian cooling and there would be no immediate reason to suspect excess argon.

Note that no excess was observed in the Hydra plagioclase megacryst nor in the cores of the other megacrysts from the other massifs (84-18A from Egersund-Ogna, 92-16/7 from Hellenen and 72b/73 from Garsaknatt). This may possibly mean that Ar did not penetrate in noticeable amount in the core of the megacrysts. So far, the recognition of excess argon remains however ambiguous. It is indeed only based on the presence of apparent ages, which are exceedingly high compared to the age obtained by independent chronometers for the emplacement of the RIC.

Samples 56/73 and 72b/73 from the Garsaknatt massif follow a similar pattern with sample 56/73 showing some of the youngest ages of any of the samples (ages as young as 455 Ma) while the staircase climbs again to ages as old as 857 Ma. Sample 72b/73 shows only one step with high ages initially followed by a low age of 556 Ma and a staircase rise to 1022 Ma. In fact, although it does not exhibit the extreme ages of the Hydra samples, 33% of the released argon yields ages older than the K–Ar and Rb–Sr ages of biotites (around 870 Ma, Verschure et al., 1980) and than the $^{40}\text{Ar}/^{39}\text{Ar}$ ages of amphiboles in the area (around 871 Ma, Bingen et al., 1998a). Given the relative difference between closure temperatures for biotite (300–360°C) (Harrison et al., 1985) and the empirical closure temperature for plagioclase (250°C) (Harrison and McDougall, 1982), this again indicates excess argon.

Finally, samples 84-18A, M88/7 and 92-16/7 from the centre of the large Egersund-Ogna body yield the lowest ages. Sample 84-18A shows no initial high and yields a simple staircase climbing to the best approach to a plateau of all the samples at 750 Ma. Sample M88/7 exhibits just one high step in both aliquots analysed followed by lows of 478 and 560 Ma and staircases leading to noisy pseudo-

plateau in the range 775 Ma though one aliquot showed ages in the final 2% of release above the intrusion age. Sample 92-16/7 exhibits only limited evidence for high initial ages followed by a staircase rise to a noisy pseudo-plateau around 870 Ma. While this is almost within the range of regional cooling, the last percent of release again exhibits very old ages.

In summary, three (0065-1/5, 0249-1/1 and 56/73) of the eight samples contain excess argon in the highest steps since they exceed the intrusion age of 930 Ma. Note that no excess was observed in the Hydra plagioclase megacryst nor in the cores of the other megacrysts from the other massifs (84-18A from Egersund-Ogna, 92-16/7 from Hellenen and 72b/73 from Garsaknatt). This may possibly mean that Ar did not penetrate in noticeable amount in the core of the megacrysts. So far, the recognition of excess argon remains however ambiguous. It is indeed only based on the presence of apparent ages, which are exceedingly high compared to the age obtained for the emplacement of the RIC, by independent chronometers.

Although often noisy, the high-temperature pseudo-plateau of the other samples fall in the range 775 to 870 Ma. All samples show the staircase increase in ages with the youngest ages generally younger than the Egersund dyke swarm at 616 ± 3 Ma, which marks the end of post-Sveconorwegian cooling. The young ages more likely reflect a Caledonian overprint rather than very slow cooling.

Arrhenius plots for ^{39}Ar stepwise release from plagioclase is shown in Fig. 4 (Table 1). Kinetic parameters were obtained from regression on the first five points (or three first points for sample 84-18A) representing our best estimate for a low temperature “domain” (Lovera et al., 1997). Although in the present experiment, the variation of potassium contents will invalidate the assumption of homogeneous initial potassium distribution used in MDD modelling (Lovera et al., 1997), we can still display the kinetic parameters of argon diffusion. The low temperature activation energies (E) for the analysed plagioclases range from 37 ± 7 to 43 ± 8 kcal/mol (excluding two outliers obtained on the samples 84-18A and 0328-31). These values are slightly lower, though within errors of 46 ± 6 kcal/mol obtained on a population of plutonic K-

feldspars (Lovera et al., 1997). This may be an indication that low temperature ^{39}Ar release is dominated by K-feldspar rather than sericite, though it is not possible to confirm this based only on the activation energy. The Arrhenius plots exhibit some similarities with ^{39}Ar from plutonic K-feldspar in that they show discontinuities, in particular in the shaded area in Fig. 5 indicates the temperature range (about 900 to 1060°C), where all plagioclases display a first break in the slope of their Arrhenius plot. Crucially, this break does not correspond simply with any variation in the age spectra. In sample 0065-1/5, the break corresponds to a slight change in the slope of ages, though in sample 0249-1/1, the ages seem to increase, perhaps because the plagioclase dominates and has more excess argon. In sample 56/73, the large jump in ages is not related to the 900–1060°C temperature range at all. Variations in the diffusion parameters derived from ^{39}Ar release from K-feldspar result from correlated release as shown by the r/r_0 plots commonly used (Lovera et al., 1997) whereas the break of slope in the plagioclase Arrhenius plots are not directly related to age variations. Thus, it seems more likely that the changes at 900 to 1060°C are related to initial sample breakdown, perhaps by reaction between the phases.

4.2. Microprobe analyses

Microprobe traverses (open circle data in Appendix A) have been obtained on three clear grains of samples 0065-1/5 and 84-18A. Continuous profiles show only two types of inclusions, a hemo-ilmenite in 0065-1/5 and a possible sericite (phengite?) in 84-18A (see Boven et al., 1996 for discussion). The mean Ca/K ratios measured by microprobe on pure plagioclase correspond reasonably with those deduced from the Ar degassed in high temperature steps. This confirms that pure plagioclase is the main phase outgassing at high temperature.

Another set of microprobe analyses (Appendix A) have been made in order to investigate on the composition of the impurities. Analyses at about 4 μm resolution were undertaken on “clear feldspar”, microcracks, mineral and/or possibly fluid inclusions, spheroid inclusions, antiperthite exsolutions. The re-

sults on “clear plagioclase” for samples 0065-1/5 and 84-18A confirm the homogeneity previously ob-

served from the microprobe traverses on the same samples (Boven et al., 1996), while large composi-

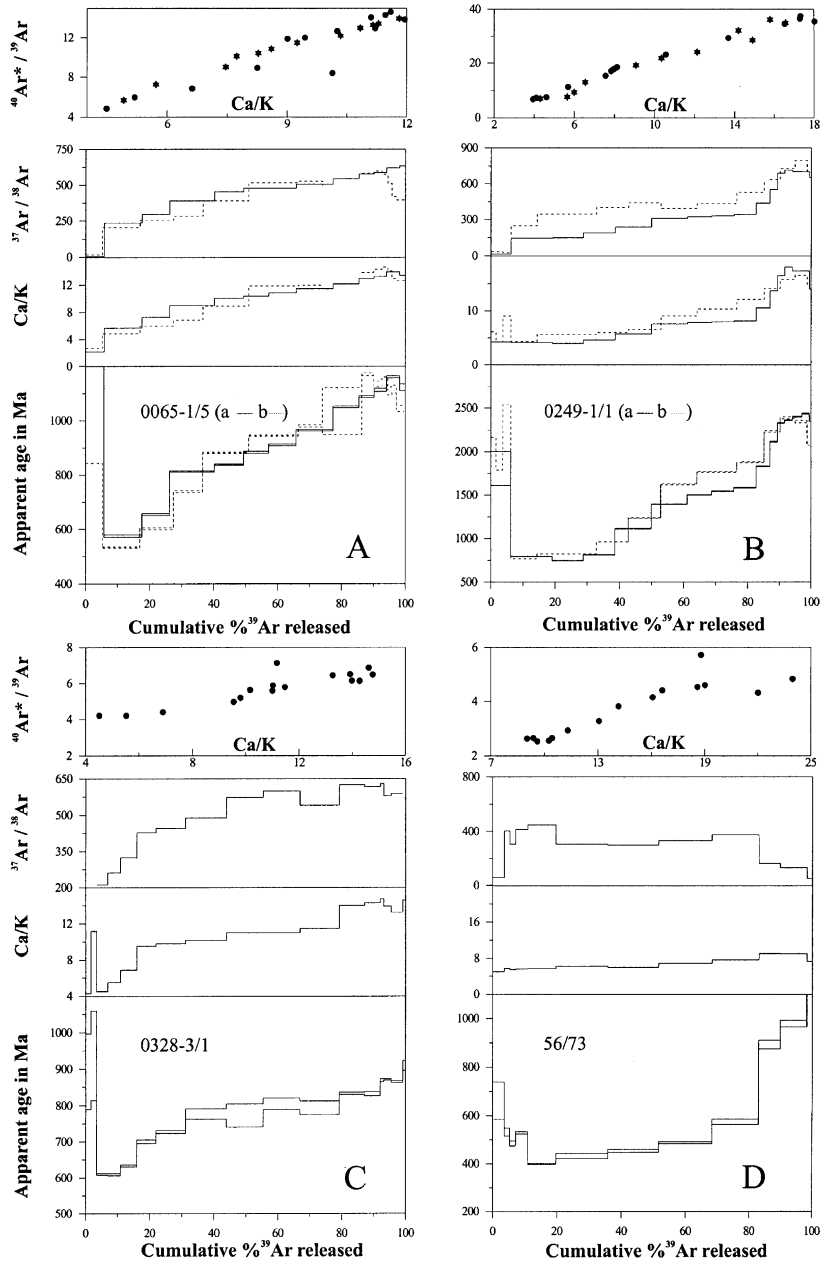


Fig. 3. A–H. Ar–Ar stepwise heating spectra of the plagioclase separates from the Rogaland Anorthosite Complex. The patterns of the apparent age, Ca/K and $^{37}\text{Ar}/^{38}\text{Ar}$ plotted against the cumulative % ^{39}Ar released are similar for most samples. The $^{40}\text{Ar}^*/^{39}\text{Ar}$ ratio vs. Ca/K shows an almost linear trend that suggests binary mixing.

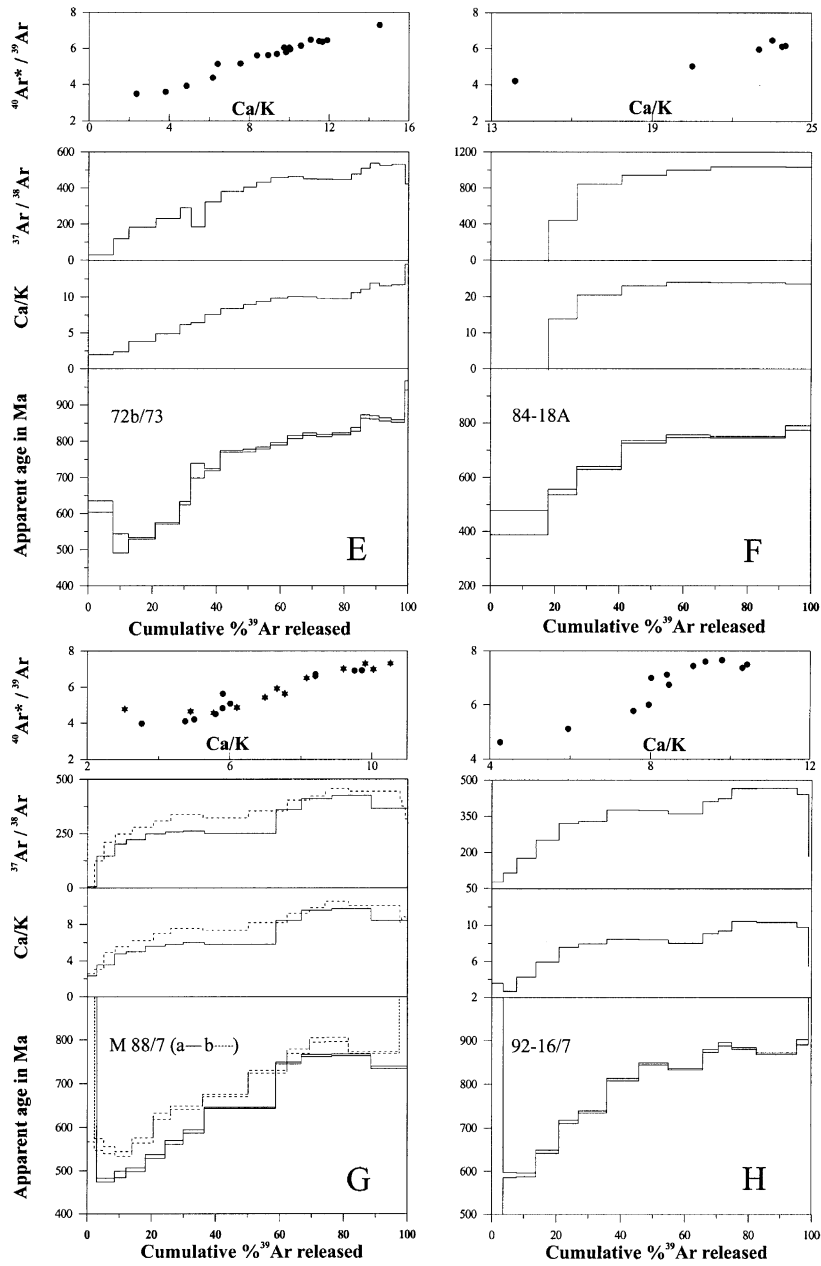


Fig. 3 (continued).

tional differences, particularly in K_2O , are observed for the wide variety of inclusions and exsolution within the plagioclase.

In most samples (except 92-16/7, 84-18A and 0328-3/1), antiperthitic lamellae were observed under the microscope. Microprobe data confirm this

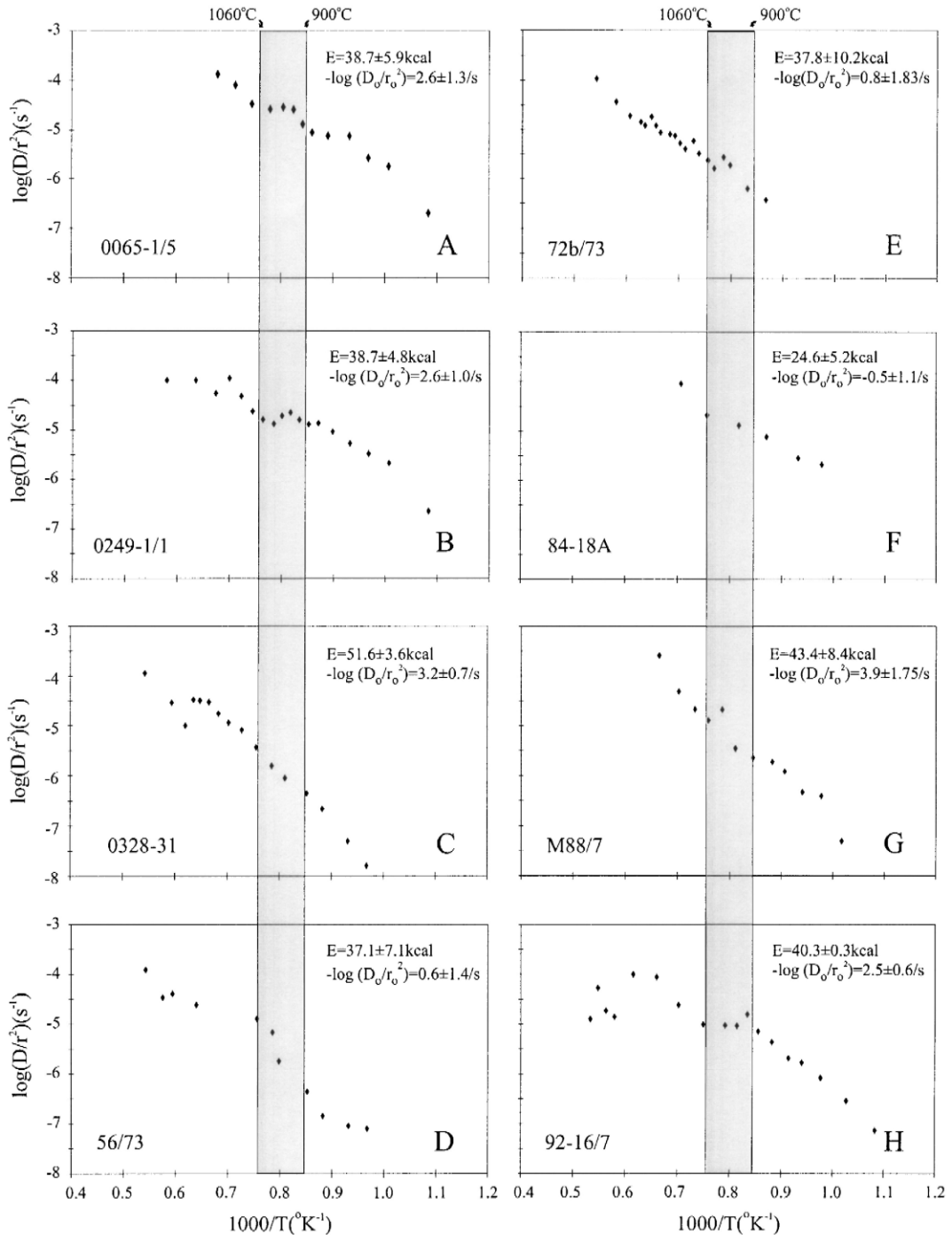


Fig. 4. A–H. Arrhenius plots for the stepwise heated plagioclase samples (20 min heating for each temperature step) from the Rogaland Anorthosite Complex. Kinetic parameters are obtained from regression on the first five points (or three first points for sample 84–18A) representing ³⁹Ar release from the lowest temperature steps. The shaded area represents the temperature range in which all plagioclase samples display a disturbance on their Arrhenius plot.

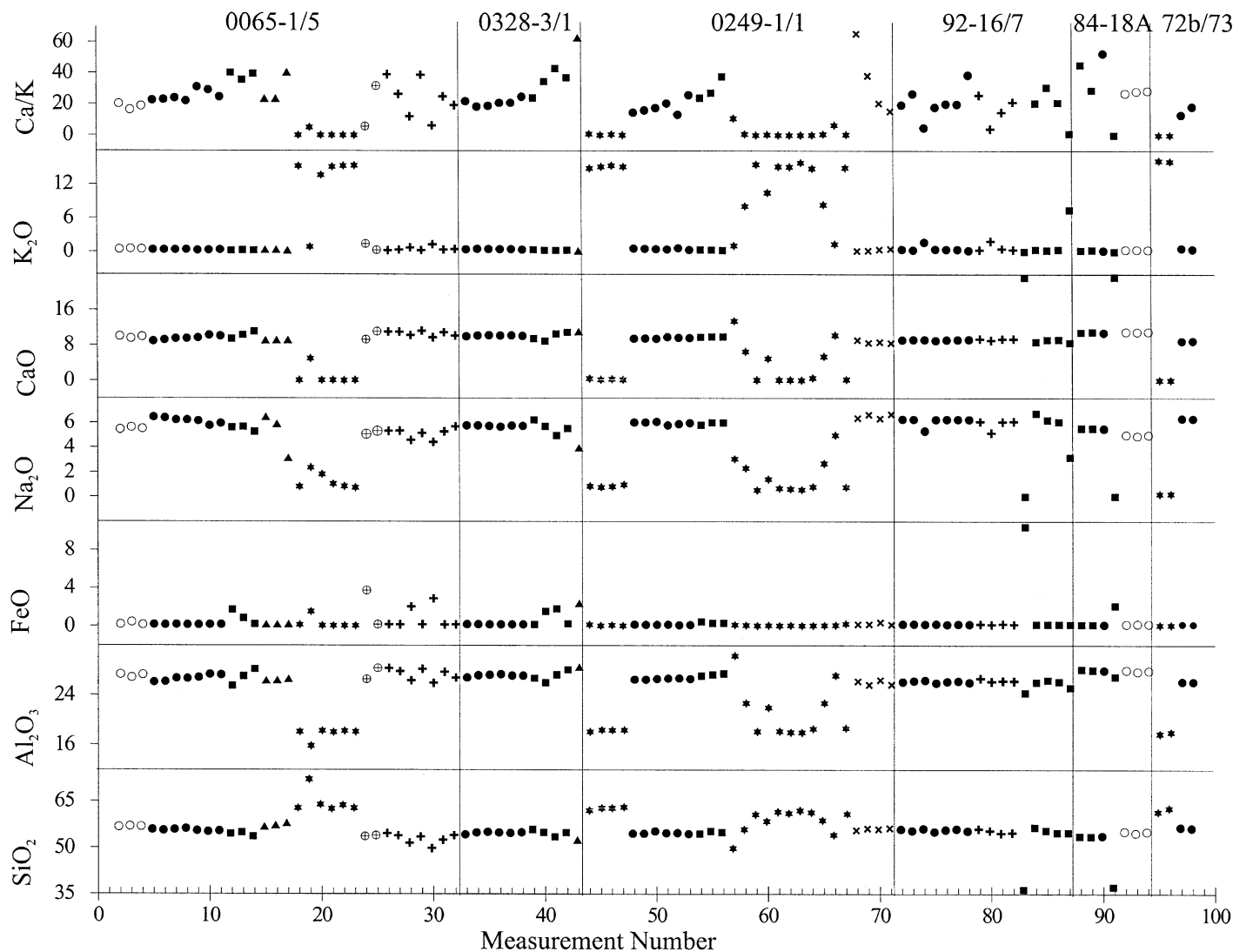


Fig. 5. Plot of the SiO_2 , Al_2O_3 , CaO , FeO , Na_2O , K_2O and Ca/K compositional variations in plagioclase samples obtained by electron microprobe analyses on clear plagioclase (●), microcrack (■), mineral inclusion (▲), spheroid mineral inclusion (⊕), antiperthite (x), clear K-spar exsolution (★) and surmised fluid inclusion (+). The open circle (○) stands for average compositions of feldspar grains (electron microprobe traverses; Boven et al., 1996). Full data set in Appendix A.

interpretation: K-feldspar is identified (see Fig. 5) in the same samples. In sample 0249-1/1, some analyses made on targets originally identified as plagioclase reveal that they actually correspond to K-

feldspar. Ca/K ratios for the antiperthitic phase show a wide range of variation. Analyses of the various types of inclusions (spheroid mineral, surmised fluid inclusions) and of the microcracks (Fig.

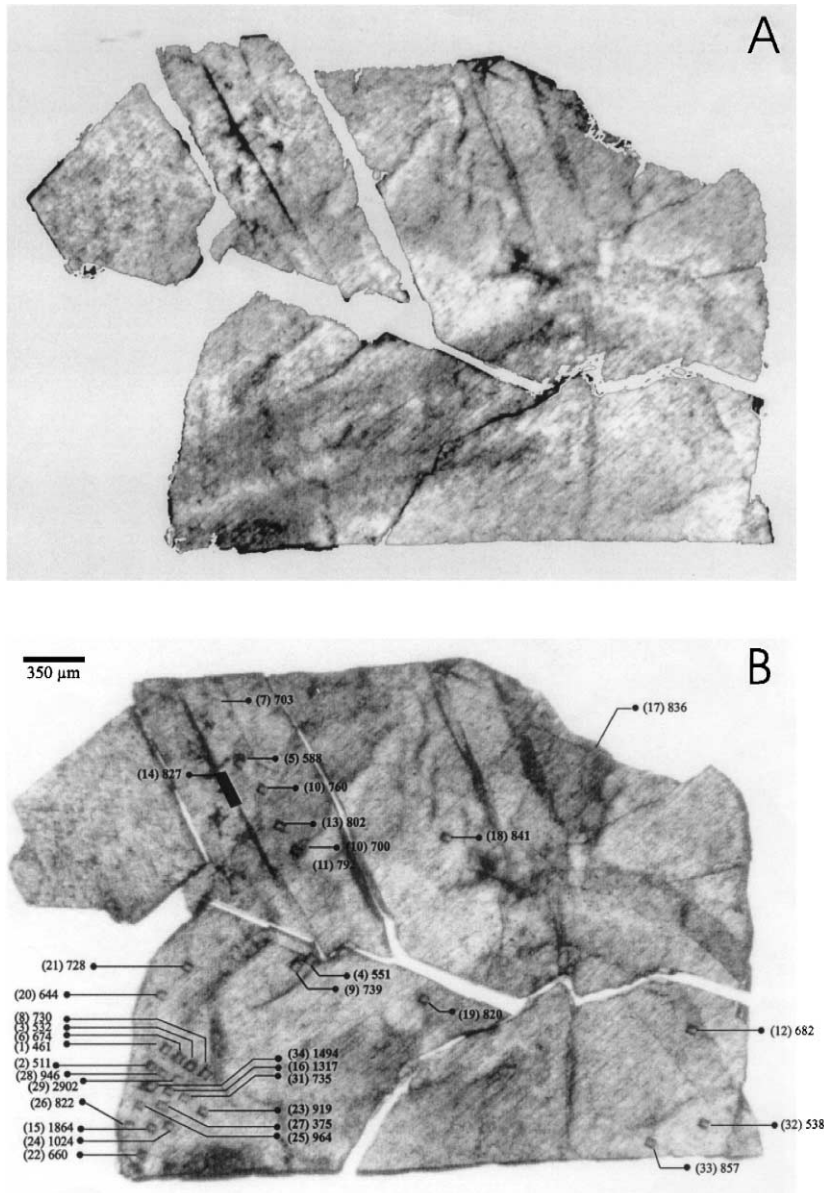


Fig. 6. (A) Photomicrograph of plagioclase 0065-1/5 prior to ablation with optically visible spheroid inclusions selected as ablation target. (B) Distribution of the UV laser ablation pits, numbers between brackets correspond to spot # in Table 2, apparent ages next to them are in Ma. Filled ablation squares have been recognized as excess argon traps (complete data set in Table 2).

5) rarely permit identification of their composition. Two analyses of microcracks (in samples 84-18A and 92-16/7) yield high CaO contents, possibly indicating the presence of a carbonate infilling. One microcrack is identified as epidote (** in sample 92-16/7, Appendix A), and another as epidote + carbonate (***) in sample 84-18A, Appendix A). Spheroid inclusions (in sample 0065-1/5, Figs. 5 and 6B), resembling those observed in the thick section of the same sample used for the $^{40}\text{Ar}/^{39}\text{Ar}$ UV-laser ablation experiment, have a composition, which is roughly that of a plagioclase, however, with K and Fe impurities. The resolution of the microprobe analyses is, however, insufficient to detect any small scale K-inhomogeneity. K–Ca feldspar inclusions have been identified in plagioclase by high-resolution transmission electron microscopy (Hoshi and Tagai, 1997). Selected-area electron diffraction patterns reveal a complex mineralogical and chemical zonation with unexsolved K-feldspar in the core of the inclusions and lamella intergrowths of K-feldspar and anorthite in the rim.

In summary, nearly all the plagioclases contain alkali feldspar exsolutions (antiperthite). They also contain other inclusions and impurities though none with high potassium contents; the sericite though observed locally is not present in sufficient quantity to explain the low bulk Ca/K ratios of the samples.

4.3. UV-laser ablation

The UV-laser ablation technique allows in-situ $^{40}\text{Ar}/^{39}\text{Ar}$ analyses at a high resolution. This technique highlights sample heterogeneity. Identification of the analysed targets within the thick (ca. 120 μm) sections used for the laser ablation technique is made by observation under reflected light with a video-camera through the laser focusing microscope. Although the resolution of the image on the monitor was poor because of imperfect polishing of the upper surface of the thick sections, the comparison with observations made under binocular under transmitted illumination together with photographs of the actual samples taken prior to irradiation allowed us to recognise minute inclusions (< 30 μm) (see Fig. 6B). The low-potassium contents of the plagioclase

mean that extraction of measurable amounts of Ar required ablation pits of at least $50 \times 50 \mu\text{m}$. The ablation craters shown on Fig. 6A are $50 \times 50 \mu\text{m}$ or in a few cases $100 \times 100 \mu\text{m}$. At this resolution the UV-laser ablation does not discriminate the different plagioclase phases but highlights heterogeneity. Because of the very low amount of argon released during the laser ablation, the Ca/K ratio derived from the argon isotopic analysis remains less precise than the stepwise-heating analyses. Around half of the UV-laser analyses were on “clear plagioclases”, others hit different kinds of inclusions. Very few laser analyses have actually been obtained on pure or nearly pure K-feldspar exsolutions, as indicated by the Ca/K ratio derived from $^{37}\text{Ar}/^{39}\text{Ar}$. The results of the analyses are presented in Table 2 in the order of increasing Ca/K ratio for each plagioclase.

The two samples from the Hydra body (0065-1/5 and 0249-1/1), which provided the clearest evidence for excess argon, also exhibit very high apparent ages in some of the UV-laser pit analyses. However, the pattern is strikingly different from stepwise-heating release, most of the ages span a range within that seen in the stepwise-heating data, from around 400 to 900 Ma (though with larger errors than the stepwise-heating analyses). Although only few analyses were undertaken in the third sample from the Hydra body (0328-3/1), ages fall in a narrow range (505 to 625 Ma) and are lower than those obtained by stepwise heating. This may be related to the cloudy and altered state of the sample analysed using the UV-laser system.

Several analyses yield high apparent ages, from 964 to 2902 Ma for sample 0065-1/5 and from 965 to 8069 Ma for sample 0249-1/1, resulting from the presence of excess argon. The latter seems to be confined to small areas, perhaps inclusions, which are highlighted by the laser but smeared out in the stepwise heating. The Ca/K ratios of the ablation targets yielding excess argon are similar to that of plagioclase.

In sample 0065-1/5, the excess argon seems most prominent in analyses of spherical mineral inclusions (see Fig. 6A, spot # 15, probably filled with fluid inclusions and spot # 24) and near these inclusions (spots # 29 and 34). The most inclusion-rich areas also exhibit low potassium, causing high errors in the resulting ages though the amounts of excess argon

were very high. None of the other samples analysed by the UV laser showed this dichotomy in ages indicating that the main source of the excess argon is confined to inclusions.

One sample from the Garsaknatt massif, 72b/73 was analysed using the UV laser and yielded ages in the range 129 to 966 Ma (Table 2), though only one age was older than the intrusion age. For the main Egersund-Ogna body, sample 84-18A yielded ages in the range 181 to 922 Ma and sample 92-16/7 in the range 397 to 753 Ma (Table 2).

5. Discussion

The relationship between the UV-laser ablation and stepwise-heating data is crucial in understanding the complex argon release from these plagioclase samples and discussion of the comparison is prefaced by a repetition of their different approaches. The UV-laser ablation extracts all gas from small areas at a high resolution. The resolution during this experiment was limited to 50×50 – 100×100 μm craters (~ 0.5 μg) in order to release measurable amounts of argon. During stepwise argon release, analyses are made on argon released sequentially from the whole sample at increasing temperatures, and the samples are generally several milligrams in weight.

The staircase-shaped argon-release patterns and Ca/K ratios seem to indicate diffusive argon loss similar to the types of patterns interpreted using the MDD model of Lovera et al., (1997 and references therein), which has previously been considered and rejected as an interpretation of similar samples (Boven et al., 1996). We will show that the situation is more complex. The role played by secondary K-bearing phases will also be discussed later. The important observation in this respect is that the stepwise-heating data show a linear correlation between Ca/K and $^{40}\text{Ar}^*/^{39}\text{Ar}$; in other words, a correlation between Ca/K and apparent age that can be interpreted as “mixing lines” resulting from the degassing of a binary assemblage with distinct Ca/K composition and ages. For example, a mixture of a plagioclase with a Sveconorwegian cooling age and

a Caledonian sericite or reset K-feldspar exsolution would result in such a $^{40}\text{Ar}^*/^{39}\text{Ar}$ vs. Ca/K mixing line. Although plagioclase is certainly one phase, there are problems in identifying the other phase in a two-component mixture.

Firstly, fine-grained sericite is present but likely to be fully outgassed above 900–1000°C (Jaboyedoff and Cosca, 1999; Müller et al., 1999). So it would not contribute to the ^{39}Ar released at higher temperatures. The samples show, however, increasing Ca/K ratios well above 1000°C. Thus, although sericite is undoubtedly present in these samples, it is unlikely to be the only factor, which generates the observed staircase age patterns.

The second possible component is K-feldspar; yet, if it is in a two-component mixture with plagioclase, it should be possible to calculate the ages of the end-members, knowing the composition of the pure plagioclase end-member (from electron microprobe analyses), and using a Ca/K ratio of zero for the potassic end-member. For example, sample 0328-3/1 (Fig. 3C) yields a zero Ca/K age of 430 Ma and a plagioclase age of 995 Ma are obtained by extrapolating the mixing line to Ca/K values of 0 and 18 (deduced from microprobe data on clear plagioclase, see Appendix A). We note, however, that the highest Ca/K value deduced from the Ar-measurements of plagioclase is slightly lower than the electron microprobe values obtained for the same plagioclases. If the higher microprobe data are used in the two-component mixing model, for all samples (except 84-18A), the high end-member ages corresponding to plagioclase (1017 to 2660 Ma), are greater than the intrusion age. In other words, this implies that either all but one of the samples contain excess argon or that the high temperature release was not from pure plagioclase.

The zero Ca/K end-members are less subject to uncertainties of composition than the high Ca end-members, yet problems arise in the calculated ages, when significant excess argon is present. For sample 0065-1/5, the zero Ca/K age (58 ± 22 Ma) is obviously too low and for 0249-1/1, it is even negative (-451 ± 42 Ma), which is obviously an artefact. The low ages of the other samples fall in the range 163 ± 44 Ma to 430 ± 14 Ma. Given the uncertainties involved, it is significant that four samples have zero Ca/K ages in agreement, within errors limits,

of the known age of Caledonian thrusting. Thus, in these limited number of cases, the data show the trend of a two-component mixture and indicate that the resetting event was associated with Caledonian thrusting. In other samples, it is more complex and it may be that even in the apparently simple cases, the two components are dominant over lesser components, which, however, become important in other samples. In particular, the effect may be caused by variable ages derived from a small K-feldspar component. K-feldspar commonly displays a range of ages as a result of subgrain size variations (Lovera et al., 1997 and references therein).

Another element, which weakens the interpretation of the data as a mixing line, lies in the UV-laser ablation results. Stepwise-heating data show a linear correlation between Ca/K and $^{40}\text{Ar}^*/^{39}\text{Ar}$, but there is no correlation between Ca/K and $^{40}\text{Ar}^*/^{39}\text{Ar}$ in the UV-laser data. In fact, the UV-laser ablation data show a wide range of ages for samples with a single Ca/K ratio (Fig. 7). This lack of correlation forces us to dismiss the simple two-component mixing hypothesis even in samples with no obvious excess argon. In fact, there must be a correlated age variation in the different components in order to explain the appearance of a correlation at all. This situation may come about if components covary in age and composition and the components release argon over similar temperature ranges producing strong mixing correlations. The fact that there is no correlation in the UV-laser ablation data indicates that K-feldspar, plagioclase or both yield variable ages. Unfortunately, the presence of even small amounts of K-feldspar mask the plagioclase ages particularly at low temperature so it is impossible to be certain that the variations result only from K-feldspar age variation. The use of plagioclase for detailed thermochronological studies may, thus, be restricted at least until plagioclase closure temperatures can be fully quantified. As mentioned above, an additional element is playing a major role in the degassing scheme of some of the plagioclase. Some of the stepwise-heating results yield steps with very high apparent ages; the UV-laser data reveals even higher ages. Those observed in stepwise heating at low temperatures (650°C) may be recoil effects (Onstott et al., 1995) associated with impurities or fluid inclusions. Those at high temperatures yield apparent

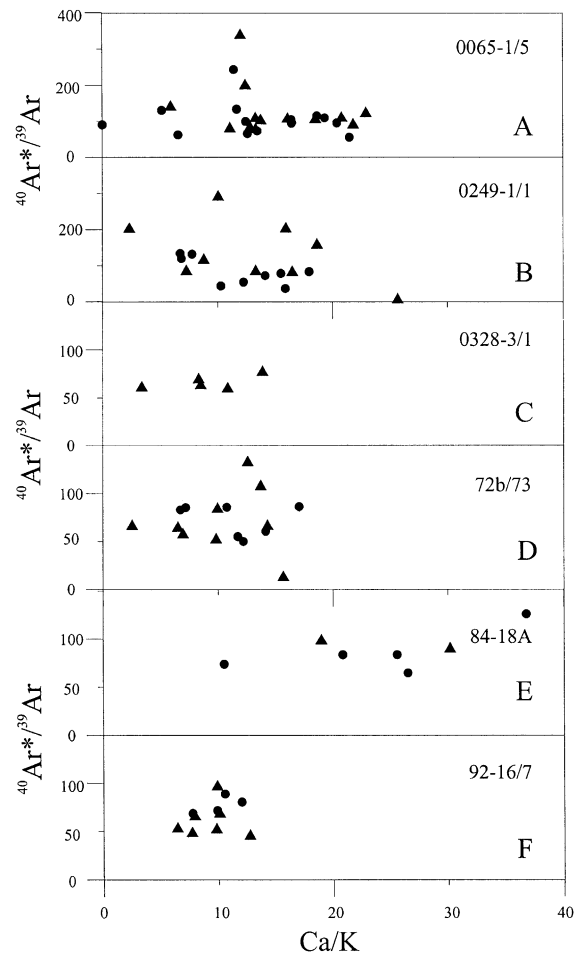


Fig. 7. Ca/K vs. $^{40}\text{Ar}^*/^{39}\text{Ar}$ UV laser ablation data on plagioclase separates. The nature of the sample for each laser spot presented in Table 2 has been grouped into (●) for clear plagioclase and (▲) for impure plagioclase or impurities (surmised fluid or mineral inclusion, microveins).

ages, which are clearly greater than the emplacement age of the RIC (930 Ma) and are, therefore, interpreted as indicative of the presence of excess argon. Three samples actually display a stepwise-heating spectra indicative for the presence of excess argon released at high temperatures. Samples (0249-1/1, 0065-1/5 and 56/73) close to K-bearing country rocks contain significant excess argon, though samples taken within the core of megacrysts in the same area (0328-3/1 and 72b/73) do not exhibit excess

argon, indicating that the argon was mobilized from the country-rock after the crystallisation of the megacrysts. The UV-laser data also show the presence of excess argon in samples for which excess argon was indicated by stepwise-heating data. The UV-laser data reveal that excess argon is actually located within inclusions, an observation concordant with the observation of several generations of high temperature fluid inclusions in the RIC (Wilmart et al., 1991, 1994). Although the specificity of the inclusions was not characterized during the present study, the highly variable ages centered around the observed inclusions is strongly indicative of excess argon residing in inclusions. The presence of inclusions in those samples where excess argon has been identified, probably affected the extrapolation of the mixing lines described earlier, skewing the high temperature high Ca/K end-member and, thus, affecting the extrapolation to the zero Ca end-member. The inclusion contribution does not suddenly appear at a certain temperature but is mixed thoroughly with argon release from the plagioclase. This indicates a homogenisation of the phases at high temperature, which probably led to plateau-like release, and to Ca/K values, which tend to be lower than for pure plagioclase.

6. Conclusions

The complexity of Ar and K migration in these well-constrained, mildly overprinted, plutonic plagioclase samples has been clearly illustrated and may provide a model for argon release from other plutonic plagioclases. In areas where plagioclase has been affected by low temperature metamorphism and/or fluid circulation, careful study by UV-laser ablation combined with conventional stepwise-heating procedure is a reasonable approach to estimate thermal histories. Although the UV-laser data showed the presence of inclusions and their importance in understanding the behaviour of excess argon, only stepped heating revealed the intimate mixing of the low Ca/K and high Ca/K phases and the presence of a Caledonian signal.

Plutonic plagioclase is best described as a multi-phase assemblage, with respect to K and Ar distributions. A simple two-component mixture may explain

much of the linear correlation seen in the present work but must be rejected in favour of a model including plagioclase, K-feldspar antiperthite, solid/fluid inclusions and sericite. The Caledonian overprint recorded by the stepwise-heating spectra in these samples originates from a combination of argon released from K-feldspar antiperthite and secondary K-rich phases, during the initial argon release. The higher step ages are in the range expected for post-Sveconorwegian cooling. Arrhenius plots indicate that argon release from the complex plagioclase system at temperatures below 900°C is dominated by a phase whose activation energy is similar to that of K-feldspar. The release mechanisms at higher temperatures are much more complex and involve mineral breakdown.

The presence of excess argon in marginal leuconorite intrusions (Garsaknatt and Hidra massifs), but not within the core of large coexisting plagioclase megacrysts, indicates that potassium and excess argon were introduced over short distances from the adjacent K-bearing country rocks (K-rich charnockites) during the cooling history of the anorthositic complex.

Acknowledgements

We thank M. Bass, R.H. Verschure and J.L. Touret for their constructive comments upon reading an earlier version of the present manuscript. An anonymous reviewer greatly helped in putting order into the ideas and his detailed review allowed us to better address the complexity of Ar release from plagioclase. O. Lovera reviewed the manuscript and N. Arnaud provided us Arrhenius data making use of O. Lovera's programs. A. Aquino and J. Van Mechele are thanked for their help in the irradiation and dosimetry analyses, A. Van de Maele for his technical assistance at the Vrije Universiteit Brussel $^{40}\text{Ar}/^{39}\text{Ar}$ laboratory. The UCL-staff in Belgium and the OU-staff in the UK for the microprobe analyses. The present work is supported by a postdoctoral FWO-fellowship to A. Boven during his stay at the Open University. This work was partly supported by a FNRS-NFWO grant to D. Demaiffe and P. Passteels.

Appendix A

SiO₂, Al₂O₃, CaO, FeO, Na₂O, K₂O and Ca/K compositional variations obtained by electron microprobe analyses on clear plagioclase (●), microcracks (■), inclusion (▲) spheroid inclusions (⊕), antiperthite (x), clear K-spar exsolutions (★) and surmised fluid inclusions (+). Open circle (○) stands for average compositions of clear feldspar grains (electron microprobe traverses). Identified minerals: * plagioclase with K, Fe impurities, ** epidote, *** epidote + carbonate.

Sample measurement number	SiO ₂ (wt.%)	Al ₂ O ₃ (wt.%)	CaO (wt.%)	FeO (wt.%)	Na ₂ O (wt.%)	K ₂ O (wt.%)	Ca/K
<i>0065-1 / 5</i>							
2 ○	56.70	27.33	10.01	0.08	5.46	0.43	20.20
3 ○	56.90	26.82	9.54	0.19	5.62	0.51	16.30
4 ○	56.80	27.26	9.93	0.07	5.51	0.45	18.80
5 ●	55.87	26.08	8.92	0.16	6.45	0.34	22.39
6 ●	55.58	26.15	9.17	0.14	6.39	0.35	22.84
7 ●	55.88	26.68	9.48	0.16	6.22	0.34	23.88
8 ●	56.14	26.66	9.52	0.14	6.22	0.37	21.92
9 ●	55.53	26.80	9.65	0.15	6.15	0.27	30.91
10 ●	55.20	27.32	10.26	0.17	5.77	0.30	29.06
11 ●	55.39	27.24	10.09	0.15	5.94	0.35	24.54
12 ■	54.48	25.50	9.47	1.72	5.62	0.20	40.20
13 ■	54.95	27.01	10.32	0.84	5.67	0.25	35.57
14 ■	53.61	28.16	11.12	0.20	5.26	0.24	39.58
15 ▲	56.75	26.30	9.07	0.17	6.45	0.33	23.40
16 ▲	57.18	26.34	9.13	0.16	5.88	0.34	23.47
17 ▲	57.84	26.56	9.12	0.17	3.14	0.20	40.30
18 ★	62.68	18.06	0.08	0.13	0.82	15.24	0.00
19 ★	71.87	15.79	5.00	1.51	2.36	0.85	5.04
20 ★	63.76	18.21	0.06	0.04	1.83	13.64	0.00
21 ★	62.42	18.01	0.08	0.02	1.04	15.13	0.00
22 ★	63.56	18.17	0.03	0.03	0.85	15.30	0.00
23 ★	62.69	18.06	0.08	0.02	0.75	15.35	0.00
24 ⊕*	53.63	26.53	9.25	3.74	5.08	1.41	5.64
25 ⊕	53.94	28.30	11.11	0.16	5.32	0.30	31.68
26 +	54.58	28.30	11.03	0.15	5.32	0.24	39.11
27 +	53.85	27.77	11.02	0.14	5.33	0.36	26.35
28 +	51.55	26.33	10.26	2.02	4.59	0.74	12.02
29 +	53.48	28.16	11.27	0.16	5.16	0.25	38.83
30 +*	49.83	25.93	9.75	2.88	4.44	1.34	6.28
31 +	52.46	27.70	10.93	0.14	5.28	0.38	24.90
32 +	53.97	26.77	10.14	0.17	5.69	0.45	19.27
<i>0328-3 / 1</i>							
33 ●	54.21	26.79	9.96	0.17	5.76	0.39	21.76
34 ●	54.86	27.15	10.14	0.17	5.76	0.48	18.28
35 ●	55.05	27.22	10.21	0.16	5.72	0.47	18.75
36 ●	54.84	27.31	10.16	0.16	5.66	0.42	20.68

37 ●	54.68	27.09	10.18	0.16	5.75	0.42	20.68
38 ●	54.88	27.10	10.08	0.16	5.73	0.35	24.67
39 ■	55.88	26.68	9.48	0.16	6.22	0.34	23.88
40 ■	54.87	25.99	8.90	1.52	5.70	0.22	34.37
41 ■	53.48	27.24	10.54	1.81	4.96	0.21	42.82
42 ■	54.86	28.02	10.91	0.22	5.52	0.25	37.00
43 ▲	52.44	28.47	11.08	2.36	3.96	0.15	62.79
<i>0249-1 / 1</i>							
44 ★	62.04	18.18	0.18	0.04	0.89	14.93	0.01
45 ★	62.73	18.32	0.18	0.04	0.90	15.12	0.01
46 ★	62.55	18.30	0.20	0.05	0.84	15.23	0.01
47 ★	62.58	18.28	0.20	0.04	0.92	15.00	0.01
48 ●	54.56	26.49	9.49	0.16	6.01	0.56	14.49
49 ●	54.53	26.48	9.52	0.14	6.02	0.52	15.93
50 ●	55.31	26.57	9.44	0.14	6.07	0.47	17.41
51 ●	54.71	26.66	9.82	0.15	5.79	0.41	20.43
52 ●	54.73	26.69	9.68	0.11	5.89	0.63	13.15
53 ●	54.43	26.58	9.62	0.13	5.97	0.32	25.82
54 ■	54.42	27.07	9.84	0.46	5.80	0.35	23.94
55 ■	55.28	27.27	9.92	0.29	6.01	0.32	27.13
56 ■	54.95	27.45	9.89	0.30	6.00	0.23	37.68
57 ★	49.74	30.32	13.50	0.12	3.06	1.08	10.81
58 ★	55.87	22.69	6.57	0.07	2.32	8.09	0.70
59 ★	60.62	18.10	0.11	0.03	0.54	15.54	0.01
60 ★	58.43	21.95	5.01	0.06	1.43	10.49	0.41
61 ★	61.48	18.14	0.11	0.03	0.69	15.15	0.01
62 ★	61.04	17.97	0.13	0.06	0.64	15.10	0.01
63 ★	61.91	17.94	0.04	0.03	0.57	15.84	0.00
64 ★	61.27	18.54	0.59	0.05	0.82	14.83	0.03
65 ★	58.74	22.71	5.45	0.07	2.69	8.35	0.56
66 ★	54.09	27.11	10.26	0.08	4.98	1.36	6.51
67 ★	60.46	18.50	0.58	0.16	0.73	14.87	0.03
68 x	55.60	26.17	9.11	0.18	6.36	0.12	65.40
69 x	56.17	25.61	8.51	0.18	6.64	0.19	38.16
70 x	55.94	26.37	8.71	0.38	6.32	0.37	20.39
71 x	56.26	25.64	8.44	0.14	6.68	0.48	15.27
<i>92-16 / 7</i>							
72 ●	55.90	26.10	9.16	0.19	6.27	0.41	19.39
73 ●	55.46	26.25	9.22	0.21	6.26	0.30	26.56
74 ●	56.12	26.36	9.21	0.18	5.33	1.68	4.72
75 ●	55.10	25.92	9.05	0.20	6.24	0.44	17.92
76 ●	55.75	26.15	9.19	0.16	6.26	0.40	20.05
77 ●	56.00	26.24	9.24	0.19	6.26	0.40	19.94
78 ●	55.37	25.99	9.25	0.18	6.25	0.21	38.66
79 +	55.99	26.66	9.45	0.19	6.09	0.32	25.75
80 +	55.46	26.16	9.13	0.17	5.18	1.92	4.10
81 +	54.64	26.24	9.46	0.20	6.07	0.55	14.78
82 +	54.79	26.22	9.44	0.18	6.10	0.38	21.28

83 ■ * *	36.39	24.33	23.24	4.00	0.01	0.00	70.00
84 ■	56.54	26.05	8.78	0.17	6.75	0.37	20.55
85 ■	55.52	26.37	9.24	0.18	6.21	0.26	30.73
86 ■	54.87	26.12	9.27	0.17	6.05	0.38	20.86
87 ■	54.78	25.16	8.55	0.16	3.19	7.41	0.99
84-18A							
88 ■	53.67	28.11	10.88	0.15	5.54	0.21	45.28
89 ■	53.57	28.01	10.97	0.15	5.55	0.33	28.90
90 ●	53.77	27.92	10.80	0.13	5.51	0.18	52.57
91 ■ * * *	37.23	26.88	23.33	2.11	0.02	0.00	0.00
92 ○	55.20	27.98	11.01	0.17	5.01	0.35	26.90
93 ○	54.70	27.73	10.96	0.21	4.93	0.34	28.10
94 ○	55.10	27.87	11.00	0.19	5.00	0.33	28.50
72b / 73							
95 ★	61.45	17.73	0.05	0.07	0.22	16.23	0.00
96 ★	62.63	17.97	0.05	0.07	0.23	16.10	0.00
97 ●	56.53	26.12	8.91	0.19	6.33	0.59	13.08
98 ●	56.26	26.09	8.94	0.16	6.31	0.42	18.28

References

- Arnaud, N.O., Kelley, S.P., 1995. Evidence for excess argon during high pressure metamorphism in the Dora Maira Massif (Western Alps, Italy), using an ultra-violet laser ablation microprobe $^{40}\text{Ar}/^{39}\text{Ar}$ technique. *Contrib. Mineral. Petrol.* 121, 249–264.
- Baksi, A.K., Archibald, D.A., Farrar, E., 1996. Intercalibration of $^{40}\text{Ar}/^{39}\text{Ar}$ dating standards. *Chem. Geol.* 129, 307–324.
- Bingen, B., van Breemen, O., 1996. U–Pb titanite geochronology in Rogaland–Vest–Agder (SW Norway): regional temperature at the time of emplacement of the Rogaland anorthosites. In: Demaiffe, D. (Ed.), *Petrology and Geochemistry of Magmatic Suites of Rocks in the Continental and Oceanic Crusts*. ULB-MRAC, Brussels, pp. 145–160.
- Bingen, B., van Breemen, O., 1998. U–Pb monazite ages in amphibolite-to granulite-facies orthogneisses reflect hydrous mineral breakdown reactions: Sveconorwegian Province of SW Norway. *Contrib. Mineral. Petrol.* 132, 336–353.
- Bingen, B., Boven, A., Punzalan, L., Wijbrans, J.R., Demaiffe, D., 1998a. Hornblende $^{40}\text{Ar}/^{39}\text{Ar}$ geochronology across terrane boundaries in the Sveconorwegian Province of S. Norway. *Precambrian Res.* 90, 159–185.
- Bingen, B., Demaiffe, D., van Breemen, O., 1998b. The 616 Ma old Egersund basaltic dike swarm, SW Norway, and late Neoproterozoic opening of Iapetus ocean. *J. Geol.* 106, 565–574.
- Boven, A., Pasteels, P., Demaiffe, D., Punzalan, L., 1996. $^{40}\text{Ar}/^{39}\text{Ar}$ release spectra on plagioclases from the Rogaland anorthosite complex (SW Norway). In: Demaiffe, D. (Ed.), *Petrology and Geochemistry of Magmatic Suites of Rocks in the Continental and Oceanic Crusts*. ULB-MRAC, Brussels, pp. 83–97.
- Dalrymple, G.B., Lanphere, M.A., 1974. $^{40}\text{Ar}/^{39}\text{Ar}$ age spectra of some undisturbed terrestrial samples. *Geochem. Cosmochim. Acta* 38, 715–738.
- Demaiffe, D., Hertogen, J., 1981. Rare earth geochemistry and strontium isotopic composition of a massif-type anorthositic–charnockitic body: the Hidra massif (Rogaland, SW Norway). *Geochim. Cosmochim. Acta* 45, 1545–1561.
- Duchesne, J.C., 1999. Fe–Ti deposits in Rogaland anorthosites (South Norway): geochemical characteristics and problems of interpretation. *Miner. Deposita* 34, 182–198.
- Duchesne, J.C., Hertogen, J., 1988. Le magma parental du lopolithe de Bjerkreim-Sokndal (Norvège Méridionale). *C. R. Acad. Sci. Paris* 306, 45–48.
- Duchesne, J.C., Roelandts, I., Demaiffe, D., Hertogen, J., Gijbels, R., De, W.J., 1974. Rare-earth data on monzonitic rocks related to anorthosites and their bearing on the nature of parental magma of the anorthositic series. *Earth Planet. Sci. Lett.* 24, 325–335.
- Duchesne, J.C., Maquil, R., Demaiffe, D., 1985a. The Rogaland anorthosites: facts and speculations. In: Tobi, A.C., Touret, J.L. (Eds.), *The Deep Proterozoic Crust in the North Atlantic Provinces*. NATO-ASI Ser., Ser. C 158. Reidel, Dordrecht, pp. 449–476.
- Duchesne, J.C., Roelandts, I., Demaiffe, D., Weis, D., 1985b. Petrogenesis of monzonitic dykes in the Egersund-Ogna anorthosite (Rogaland, SW Norway); trace elements and isotopic (Sr, Pb) constraints. *Contrib. Mineral. Petrol.* 90, 214–225.

- Esser, R.P., McIntosh, W.C., Heizler, M.T., Kyle, P.R., 1997. Excess argon in melt inclusions in zero-age anorthoclase feldspar from Mt. Erebus, Antarctica, as revealed by the $^{40}\text{Ar}/^{39}\text{Ar}$ method. *Geochim. Cosmochim. Acta* 61, 3789–3801.
- Fram, M.S., Longhi, J., 1992. Phase equilibria of dikes associated with Proterozoic anorthosite complexes. *Am. Mineral.* 77, 605–616.
- Harrison, T.M., McDougall, I., 1981. Excess ^{40}Ar in metamorphic rocks from Broken Hill, New South Wales; implications for $^{40}\text{Ar}/^{39}\text{Ar}$ age spectra and the thermal history of the region. *Earth Planet. Sci. Lett.* 55, 123–149.
- Harrison, T.M., McDougall, I., 1982. The thermal significance of potassium feldspar K–Ar ages inferred from $^{40}\text{Ar}/^{39}\text{Ar}$ age spectrum results. *Geochim. Cosmochim. Acta* 46, 1811–1820.
- Harrison, T.M., Duncan, I., McDougall, I., 1985. Diffusion of ^{40}Ar in biotite; temperature, pressure and compositional effects. *Geochim. Cosmochim. Acta* 49, 2461–2468.
- Hess, J.C., Lippolt, H.J., 1994. Compilation of K–Ar measurements on HD-B1 standard biotite; 1994 status report. *Bulletin of Liaison and Informations, IGCP Project 196, Calibration of the Phanerozoic Time Scale*, 19–23.
- Hoshi, T., Tagai, T., 1997. TEM investigation of potassium–calcium feldspar inclusions on Bøggild plagioclase. *Am. Mineral.* 82, 1073–1078.
- Izett, G.A., Dalrymple, G.B., Snee, L., 1992. $^{40}\text{Ar}/^{39}\text{Ar}$ ages of the Cretaceous–Tertiary boundary tektites from Haiti. *Science* 252, 1539–1542.
- Jaboyedoff, M., Cosca, M.A., 1999. Dating incipient metamorphism using $^{40}\text{Ar}/^{39}\text{Ar}$ geochronology and XRD modeling; a case study from the Swiss Alps. *Contrib. Mineral. Petrol.* 135, 93–113.
- Lanphere, M.A., Dalrymple, G.B., 1976. Identification of excess ^{40}Ar by $^{40}\text{Ar}/^{39}\text{Ar}$ spectrum techniques. *Earth Planet. Sci. Lett.* 32, 141–148.
- Lo Bello, P., Feraud, G., Hall, C.M., York, D., Lavina, P., Bernat, M., 1987. $^{40}\text{Ar}/^{39}\text{Ar}$ step-heating and laser fusion dating of a Quaternary pumice from Neschers, Massif Central, France; the defeat of xenocrystic contamination. *Chem. Geol.; Isot. Geosci. Section* 66, 61–71.
- Longhi, J., Fram, M.S., Vander Auwera, J., Montieth, J.N., 1993. Pressure effects, kinetics, and rheology of anorthositic and related magmas. *Am. Mineral.* 78, 1016–1030.
- Lovera, O.M., Richter, F.M., Harrison, T.M., 1989. $^{40}\text{Ar}/^{39}\text{Ar}$ thermochronometry for slowly cooled samples having a distribution of diffusion domain sizes. *J. Geophys. Res.* 94, 17917–17935.
- Lovera, O.M., Grove, M., Harrison, T.M., Mahon, K.I., 1997. Systematic analysis of K-feldspar $^{40}\text{Ar}/^{39}\text{Ar}$ step heating results: I. Significance of activation energy determinations. *Geochim. Cosmochim. Acta* 61, 3171–3192.
- Maijer, C., 1996. Exsolution and decomposition of high-temperature feldspars from Rogaland, SW Norway. In: Demaiffe, D. (Ed.), *Petrology and Geochemistry of Magmatic Suites of Rocks in the Continental and Oceanic Crusts*. ULB-MRAC, Brussels, pp. 99–110.
- Michot, J., Michot, P., 1969. The problem of anorthosites; the south-Rogaland igneous complex, southwestern Norway. *Mem. N. Y. State Mus. Sci. Serv.* 399–410.
- Müller, W., Dallmeyer, R.D., Neubauer, F., Thöni, M., 1999. Deformation-induced resetting of Rb/Sr and $^{40}\text{Ar}/^{39}\text{Ar}$ mineral systems in a low-grade, polymetamorphic terrane (Eastern Alps, Austria). *J. Geol. Soc. (London)* 156, 261–278, Part 2.
- Onstott, T.C., Miller, M.L., Ewing, R.C., Arnold, G.W., Walsh, D.S., 1995. Recoil refinements; implications for the $^{40}\text{Ar}/^{39}\text{Ar}$ dating technique. *Geochim. Cosmochim. Acta* 59, 1821–1834.
- Parsons, I., Brown, W.L., Smith, J.V., 1999. $^{40}\text{Ar}/^{39}\text{Ar}$ thermochronology using alkali feldspars: real thermal history or mathematical mirage of microtexture? *Contrib. Mineral. Petrol.* 136 (1), 92–110.
- Pasteels, P., Michot, J., 1975. Geochronologic investigation of the metamorphic terrain of southwestern Norway. *Norsk Geol. Tidsskr.* 55, 111–134.
- Pasteels, P., Demaiffe, D., Michot, J., 1979. U–Pb and Rb–Sr geochronology of the eastern part of the South Rogaland igneous complex, southern Norway. *Lithos* 12, 199–208.
- Pidgeon, R.T., Bosch, D., Bruguier, O., 1996. Inherited zircon and titanite U–Pb systems in an Archaean syenite from southwestern Australia; implications for U–Pb stability of titanite. *Earth Planet. Sci. Lett.* 141, 187–198.
- Renne, P.R., Swisher III, C.C., Deino, A.L., Karner, D.B., Owens, T.L., DePaolo, D.J., 1998. Intercalibration of standards, absolute ages and uncertainties in $^{40}\text{Ar}/^{39}\text{Ar}$ dating. *Chem. Geol., Isot. Geosci. Section* 145, 117–152.
- Robins, B., Tumyr, O., Tysseland, M., Garmann, L.B., 1997. The Bjerkreim-Sokndal layered intrusion, Rogaland, SW Norway: evidence from marginal rocks for a jotunite parent magma. *Lithos* 39, 121–133.
- Roselieb, K., Blanc, P., Buettner, H., Jambon, A., Rammensee, W., Rosenhauer, M., Vielzeuf, D., Walter, H., 1997. Experimental study of argon sorption in quartz; evidence for argon incompatibility. *Geochim. Cosmochim. Acta* 61, 533–542.
- Sauter, P.C.C., Hermans, G.A.E.M., Jansen, J.B.H., Maijer, C., Spits, P., Wegelin, A., 1983. Polyphase Caledonian metamorphism in the Precambrian basement of Rogaland/Vest Agder, SW Norway. *Nor. Geol. Unders. Bull.* 380, 7–22.
- Schärer, U., Wilmart, E., Duchesne, J.C., 1996. The short duration and anorogenic character of anorthosite magmatism; U–Pb dating of the Rogaland Complex, Norway. *Earth Planet. Sci. Lett.* 139, 335–350.
- Sigmond, E.M.O., Gustavson, M., Roberts, D., 1984. Berggrunnskart over Norge, 1:1 million. *Nor. Geol. Unders.* .
- Singer, B.S., Pringle, M.S., 1996. Age and duration of the Matuyama–Brunhes geomagnetic polarity reversal from $^{40}\text{Ar}/^{39}\text{Ar}$ incremental heating analyses of lavas. *Earth Planet. Sci. Lett.* 139, 47–61.
- Singer, B.S., Wijbrans, J.R., Nelson, S.T., Pringle, M.S., Feeley, T.C., Dungan, M.A., 1998. Inherited argon in a Pleistocene andesite lava; $^{40}\text{Ar}/^{39}\text{Ar}$ incremental-heating and laser-fusion analyses of plagioclase. *Geology (Boulder)* 26, 427–430.
- Smith, J.V., 1984. Phase relations of plagioclase feldspars. In: Brown, W.L. (Ed.), *Feldspars Feldspathoids*. Reidel, Dordrecht, pp. 55–94, Series C.
- Tobi, A.C., Hermans, G.A.E.M., Maijer, C., Jansen, J.B.H., 1985.

- Metamorphic zoning in the high-grade Proterozoic of Rogaland-Vest Agder, SW Norway. NATO-ASI Ser., Ser. C 158. Reidel, Dordrecht, pp. 477–497.
- Van den haute, P., 1977. Apatite fission track dating of Precambrian intrusive rocks from the southern Rogaland (South-western Norway). *Bull. Soc. Belge Geol.* 86, 97–110, Bulletin van de Belgische Vereniging voor Geologie.
- Verschure, R.H., Andriessen, P.A.M., Boelrijk, N.A.I.M., Hebeda, E.H., Maijer, C., Priem, H.N.A., Verdurmen, E.A.T., 1980. On the thermal stability of Rb–Sr and K–Ar biotite systems; evidence from coexisting Sveconorwegian (ca 870 Ma) and Caledonian (ca 400 Ma) biotites in SW Norway. *Contrib. Mineral. Petrol.* 74, 245–252.
- Villa, I.M., Grobety, B., Kelley, S.P., Trigila, R., Wieler, R., 1996. Assessing Ar transport paths and mechanisms in the McClure Mountains hornblende. *Contrib. Mineral. Petrol.* 126, 67–80.
- Wielens, J.B.W., Andriessen, P.A.M., Boelrijk, N.A.I.M., Hebeda, E.H., Priem, H.N.A., Verdurmen, E.A.T., Verschure, R.H., 1981. Isotope geochronology in the high-grade metamorphic Precambrian of southwestern Norway: new data and reinterpretations. *Nor. Geol. Unders. Bull.* 359, 1–30.
- Wilmart, E., Clocchiatti, R., Duchesne, J.C., Touret, J.L.R., 1991. Fluid inclusions in charnockites from the Bjerkreim-Sokndal massif (Rogaland, southwestern Norway); fluid origin and in situ evolution. *Contrib. Mineral. Petrol.* 108, 453–462.
- Wilmart, E., Pineau, F., Rejou, M.A., Duchesne, J.C., 1994. Fluid transfer in anorthosites and related rocks from Rogaland (Southwest Norway); evidence from stable isotopes. *Earth Planet. Sci. Lett.* 125, 55–70.
- Yu, Y., Morse, S.A., 1992. Age and cooling history of the Kiglapait Intrusion from an $^{40}\text{Ar}/^{39}\text{Ar}$ study. *Geochim. Cosmochim. Acta* 56, 2471–2485.
- Zhang, L., Schärer, U., 1996. Inherited Pb components in magmatic titanite and their consequence for the interpretation of U–Pb ages. *Earth Planet. Sci. Lett.* 138, 57–65.